Copyright © 2026 Emerald Publishing Limited. This author accepted manuscript is deposited under a Creative Commons Attribution Non-commercial 4.0 International (CC BY-NC) licence. This means that anyone may distribute, adapt, and build upon the work for non-commercial purposes, subject to full attribution. If you wish to use this manuscript for commercial purposes, please contact permissions@emerald.com (see: https://www.emeraldgrouppublishing.com/publish-with-us/author-policies/our-open-research-policies#green).

Lateral-torsional buckling of HSS I-beams: design, parameter and reliability analysis

Ikram Abarkan[a], Musab Rabi[b], Felipe Piana Vendramell Ferreira*[c], Rabee Shamass[d], Konstantinos Daniel Tsavdaridis[e]

[a] Department of Physics, Faculty of Sciences, Abdelmalek Essaâdi University, 93002, Tetouan, Morocco.

[b] Department of Civil Engineering, Jerash University, 26150, Jordan.

[c] Department of Civil Engineering, State University of Maringá, Maringá, Paraná, Brazil.

[d] Civil and Environmental Engineering Department, Brunel University of London, London, UK.

[e] Department of Engineering, School of Science & Technology, City St George's, University of London, Northampton Square, EC1V 0HB, London, UK.

Abstract

This paper aims to examine the resistance of HSS doubly symmetric I-beams according to BS EN 1993-1-1, ANSI/AISC 360-22, and AS 4100-1998 (R2020). For this purpose, a database comprising 138 tests conducted between 1969 and 2023 was compiled. An influence parameter analysis was performed using the collected data, followed by a reliability assessment. The parametric influence analysis showed that geometric properties (depth, flange width, and thickness) govern bending resistance, whereas material strength plays a secondary role within the investigated range. These findings clarify the relative performance of current design provisions, highlight the parameters that most affect resistance, and indicate where refinements may improve the reliability and accuracy of HSS I-beam design. All three standards underestimate the bending resistance of HSS I-beams, though to different degrees. Among the evaluated formulations, the BS EN 1993-1-1 New Method with refinements by Tankova *et al.* achieved the highest accuracy, while ANSI/AISC 360-22 provided the least conservative predictions and AS 4100-1998 (R2020) showed moderate conservatism. The reliability analysis confirmed these trends, with partial safety factors ranging from 1.423 to 1.490, indicating systematic differences in safety margins between codes.

Keywords: High-strength steel; Tests; Design codes; Parameter influence; Reliability analysis.

*Corresponding author: fpvferreira@uem.br (Felipe Piana Vendramell Ferreira);

Notation list

A_i: cross-sectional area for the calculation of the characteristic resistance to an axial force

b: mean value correction factor

b_f: flange width

C_b: lateral-torsional buckling modification factor for non-uniform moment diagrams when both ends of the segment are braced

C_w: warping constant

CoV: coefficient of variation

E: modulus of elasticity

f_M: modification factor for LTB

f_y: yield strength of steel

$f_{y,flange}$: yield strength of the flange

$f_{y,web}$: yield strength of the web

h: steel section depth

h_w: web depth

I_y, I_z: moment of inertia about strong and weak axes, respectively

J: torsional constant

k_c: coefficient for slender unstiffened elements

$k_{d,n}$: design fractile factor for finite sample size

$k_{d,\infty}$: design fractile factor for $n \rightarrow \infty$

k_l: factor for load height

k_n: characteristic fractile factor for finite sample size

k_r: factor for restraint against lateral rotation

k_t: factor for twist restraints

k_∞: characteristic fractile factor for $n \rightarrow \infty$

L_b: umbraced length

L_p: limiting laterally unbraced length for the limit state of yielding

L_r: limiting laterally unbraced length for the limit state of inelastic lateral-torsional buckling

L_z: buckling length

l_e: effective length of a laterally unrestrained member

MAE: Mean Absolute Error

M_A: absolute value of moment at quarter point of the unbraced segment

M_B: absolute value of moment at centreline of the unbraced segment

M_C: absolute value of moment at three-quarter point of the unbraced segment

M_{cr}: elastic critical moment for lateral torsional buckling

$M_{cr,0}$: basic elastic critical moment for LTB

M_{max}: absolute value of maximum moment in the unbraced segment

M_{nf}: nominal flexural strength of the flange

$M_{n,LTB}$: nominal lateral-torsional buckling strength

M_o: elastic buckling moment for a member subject to bending

M_{pl}: plastic moment

M_{Reg}: predicted resistance based on regression model for HSS I-beams

M_{Rd}: design value of the LTB moment resistance

M_{Rk}: characteristic value of the bending moment resistance

M_s: nominal section moment capacity

M_{TEST}: moment resistance of the test

M_{nw}: nominal flexural strength of the web

N_{cry}, N_{crz}: elastic critical axial force for flexural buckling about strong and weak axes, respectively

n: number of experimental resultsR^2: coefficient of determination

r_d: design resistance

$r_{e,i}$: experimental resistance

r_k: characteristic resistance

RMSE: Root Mean Square Error

$r_{t,i}$: theoretical resistance

r_z: radius of gyration about weak axis

SD: standard deviation

SAi: sensitivity index of parameter i on the predicted resistance

s_Δ: standard deviation of the logarithmic error term

s_Δ^2: variance of the logarithmic error term

t_f: flange thickness

t_w: web thickness

V_r: coefficient of variation of resistance

V_{rt}: coefficient of variation of the theoretical resistance

V_{Xi}: coefficient of variation for yield strength of steel

V_δ: coefficient of variation of the error term

W_{el}: elastic section modulus

$W_{el,y}$, $W_{el,z}$: elastic section modulus for bending about strong and weak axes, respectively

$W_{pl,y}$, $W_{pl,z}$: plastic section modulus for bending about strong and weak axes, respectively

W_y: section modulus about the strong axis

X_m: mean value of the basic variables

α_{LT}: imperfection factor for lateral torsional buckling

α_m: moment modification factor for bending

α_s: slenderness reduction factor

γ_{M0}: partial factor for resistance of cross-sections

Δ: logarithm of the error term

$\overline{\Delta}$: mean value of the logarithmic error term

δ_i: error result for test $i\varepsilon$: material parameter depending on f_y

$\bar{\lambda}_{LT}$: relative slenderness for lateral torsional buckling

$\bar{\lambda}_{LT,0}$: plateau length of the lateral torsional buckling curves

λ_{ef}: plate element slenderness of the flange

λ_{ep}: plate element plasticity slenderness limit

λ_{ew}: plate element slenderness of the web

λ_{ey}: plate element yield slenderness limit

λ_{rw}: limiting width-to-thickness ratio for noncompact web

λ_{rf}: limiting width-to-thickness ratio for noncompact flange

λ_s: section slenderness

λ_z: relative slenderness for flexural buckling about the weak axis

ϕ_{LT}: value to determine the reduction factor χ_{LT} for lateral torsional buckling

χ_{LT}: reduction factor for lateral torsional buckling

1. Introduction

High-strength steels (HSS) are characterised by a minimum yield strength (f_y) of 460 MPa. Their use has been growing in various regions of the world, primarily due to cost-effectiveness and sustainability benefits. HSS require a reduced amount of material to achieve the same performance as conventional steels, offer enhanced corrosion resistance, which contributes to greater durability, and require less maintenance (Bjorhovde, 2004; Karabulut *et al.*, 2021; Miki *et al.*, 2002; Rabi *et al.*, 2023, 2024; Shi *et al.*, 2016; Veljkovic and Johansson, 2004; Wheeler and Russell, 2005). Using HSS allows for the creation of lightweight structures, leading to significant weight reduction. By utilising HSS, weight savings of up to 34% can be achieved (Mela and Heinisuo, 2014). A lighter structure typically requires smaller foundations and shortens both construction and transportation times, helping to reduce costs, CO_2 emissions, and energy consumption (Zhu *et al.*, 2023).

The structural behaviour of steel I-beams bending about their strong axis is well established in the literature. The resistance of these elements can be governed by yielding, local buckling (LB) and lateral-torsional buckling (LTB). The latter is characterised by a combination of vertical and lateral deflections with torsion, caused by the absence of lateral bracing along the compressed flange. LTB is particularly important in designs lacking lateral bracing and in situations where the lateral bracing system has not yet been fully installed. Most accidents occur while lateral braces are being installed, since there is an increase in variable actions (Galambos and Surovek, 2008). HSS structures have a lower rotational capacity compared to those made from conventional steels, and this capacity tends to decrease as the slenderness of the web and upper flange increases. As a result, failure may occur due to local buckling modes (Ricles *et al.*, 1998).

161 One of the first published studies was carried out by McDermott (1969). In this study, seven
162 beams with simple supports were tested under a uniform moment, while two beams were
163 subjected to a moment gradient. Tests on both uniform moment beams and gradient moment
164 beams showed that HSS has adequate rotation capacity for use in plastically designed structures.
165 However, the tests also indicated the potential for early plastic buckling. In Dibley (1969),
166 twenty-five tests were conducted to examine the behaviour of HSS under LTB. The author
167 highlighted that HSS beams under LTB showed higher resistance due to the hardening effect.
168 Beg and Hladnik (1996) tested ten HSS I-beams under four-point bending with lateral restraints
169 at the load points, to assess the flange slenderness limit. All beams failed due to LTB. Green *et*
170 *al.* (2002), flexural tests were conducted on HSS I-beams, and the results indicated that HSS
171 exhibits lower rotational resistance compared to common steels. Lee *et al.* (2013) tested sixteen
172 specimens to investigate the effect of flange slenderness on flexural strength and the rotational
173 capacity of HSS beams. Although lateral braces were considered along the span, five specimens
174 had the failure mode governed by the LTB.

175 In Xiong *et al*. (2016), eight specimens were subjected to three-point bending to study LTB
176 resistance, with lateral braces at mid-span. All models failed due to LTB, showing two-wave
177 deformation patterns. A subsequent parametric study, using the same boundary conditions,
178 revealed that predictions from ANSI/AISC 360-10 (2010) were not conservative. In contrast,
179 comparisons with the buckling curves from BS EN 1993-1-1 (2002) generally showed
180 conservative results, with resistance values exceeding buckling curve ‘a’. Xiong *et al*. (2021)
181 applied a similar methodology in relation to the previous study. However, the authors did not
182 consider lateral braces at mid-span. All eight models tested had the failure mode characterised
183 by LTB. Yang *et al*. (2019) performed eight three-point bending tests, with all specimens failing
184 due to LTB. A subsequent finite element parametric study showed that as the slenderness or the

depth-to-width ratio of the cross-section increases, resistance to LTB decreases. Luo *et al*. (2020) evaluated the behaviour of I-beams at both room and high temperatures through testing. The specimen tested at room temperature failed due to overall buckling and material strength. In Le *et al*. (2020) eight tests were conducted to assess the buckling behaviour of beams, which were simply supported and submitted to three and four-point bending with lateral braces at loading points. Six specimens failed due to LTB, linked to partial yielding, as buckling occurred in the compressed flange in the non-linear stress-strain regime. They found that BS EN 1993-1-1 (2002) buckling curve 'd' was less conservative for stocky beams but conservative for slender beams. ANSI/AISC 360-16 (2016) overestimated the results, while AS 4100-1998 (R2020) provided accurate predictions for stocky beams but conservative ones for slender beams. In Yan *et al*. (2020), four HSS welded I-section beams were tested under uniform moment with lateral braces, and all specimens failed due to LTB. The authors noted that ANSI/AISC 360-16 (2016) offered accurate predictions for the moment capacities of beams, while BS EN 1993-1-1 (2002) was more conservative. In Wang *et al.* (2021), eighteen partially restrained beams were tested to examine their LTB resistance. The authors emphasised the need to enhance the design recommendations of BS EN 1993-1-1 (2002) to address the LTB of partially restrained beams, as the buckling curve 'd' for welded sections presented conservative results compared to the test outcomes. In Tankova *et al.* (2021), twelve simply supported beams with lateral braces were tested under four-point bending, including both hybrid and homogeneous sections. All specimens failed due to LTB. When comparing the results with BS BS EN 1993-1-1 (2002), significant differences were observed, as the code underestimated the resistance to LTB. Xiong *et al.* (2022) tested eleven specimens to assess the LTB resistance of steel I-beams with double lateral braces under four-point bending. The findings revealed that LTB resistance was greater than the provisions predicted by BS EN 1993-1-1 (2002) and ANSI/AISC 360-16 (2010). Zhu *et al*. (2023) carried out tests on HSS I-beams using a restraint

system to prevent LTB and showed that the slenderness limits in BS EN 1993-1-1 (2022), for Class 2 and Class 3, were appropriate for classifying the outstand flange and web.

Residual stresses arise in steel profiles due to non-uniform heating and cooling during manufacturing, affecting both rolled and welded members (Alpsten, 1968). These stresses influence buckling resistance by triggering inelastic behaviour at stress levels below the yield strength (Alpsten and Tall, 1970; Nagaraja Rao *et al.*, 1964; Young, 1975), resulting in a non-linear stress-strain response (Huber and Beedle, 1954). In high-strength steels, welded sections dominate, and consequently, relatively limited information exists on residual stress distributions in hot-rolled HSS profiles. Dibley (1969)'s measurements indicated that rolled HSS sections exhibit residual stresses comparable in magnitude and distribution to those in lower-strength steels. Existing studies show that residual stresses have a smaller effect on the buckling resistance of welded HSS than on conventional steels (Sabau *et al.*, 2020; Tall, 1961) and that their influence does not increase with yield strength (Jönsson and Stan, 2017; Lee *et al.*, 2013). Several models have been proposed to characterise residual stresses in hot-rolled sections, including linear formulations (Galambos and Ketter, 1959; Huber and Beedle, 1954; Spoorenberg *et al.*, 2011) and parabolic models (Beer and Schultz, 1970; Szalai and Papp, 2005; Young, 1975). In contrast, a broader range of studies is available for welded sections across different steel grades (Ban *et al.*, 2013; Li *et al.*, 2015; Schaper *et al.*, 2022; Su *et al.*, 2021; Wang and Qin, 2016; Yang *et al.*, 2016).

In parallel with these findings, numerous experimental investigations have been carried out to evaluate the resistance of HSS I-beams, particularly with respect to lateral-torsional buckling behaviour, revealing that current design codes do not accurately predict their resistance. As discussed previously, several studies reported that code-based provisions either underestimate or inconsistently capture the observed resistance, even when lateral restraints are provided. The

234 design codes mentioned above adopt different modelling assumptions and, consequently,
235 distinct resistance curves, which explicitly account for imperfections such as residual stresses.
236 Another key aspect influencing these predictions is the yield strength range considered in each
237 of these procedures. For example, the yield strength limits addressed by BS EN 1993-1-1
238 (2022), ANSI/AISC 360-22 and AS 4100-1998 (R2020) are, respectively, $235 \leq f_y \leq 700$,
239 $250 \leq f_y \leq 450$ and $230 \leq f_y \leq 690$ in MPa.

240 Despite the breadth of available experimental evidence, a comprehensive assessment that
241 consistently evaluates these design approaches against a unified experimental database remains
242 limited. In this context, this paper aims to evaluate the resistance of HSS doubly symmetric I-
243 beams, in accordance with AS 4100-1998 (R2020), ANSI/AISC 360-22 and BS EN 1993-1-1
244 (2022) , using one hundred and thirty-eight tests performed between 1969 and 2023. A
245 parameter influence analysis is carried out based on the collected data, followed by a reliability
246 analysis.

247 It is important to emphasise that the tests included in the database, presented in section 2,
248 incorporate real geometric and material imperfections, unlike the simplified imperfection
249 models typically adopted in international design codes. Therefore, this study distinguishes itself
250 by directly comparing experimentally obtained results under real imperfection conditions with
251 code-based predictions, offering a more representative and original contribution to the
252 assessment of structural behaviour.

253

254 **2. Database**

255 A total of 138 data from fifteen references (Beg and Hladnik, 1996; Dibley, 1969; Le *et al.*,
256 2020; Lee *et al.*, 2013; Luo *et al.*, 2020; McDermott, 1969; Tankova *et al.*, 2021; Wang *et al.*,

2021; Xiong *et al.*, 2016, 2021, 2022; Yan *et al.*, 2020; Yang *et al.*, 2019; Zhu *et al.*, 2023) covering the years from 1969 to 2023, on the resistance HSS doubly symmetric I-beams were collected, in which the key parameters include the depth (h), the flange width (b_f), the flange thickness (t_f), the web thickness (t_w), the unbraced length (L_b), defined as the clear distance between lateral restraints, the yield strength of the flange ($f_{y,flange}$), the yield strength of the web ($f_{y,web}$) and the resistance (M_{TEST}). The following the inclusion and exclusion rules are presented:

Inclusion rules:

- Test on doubly symmetric I-section beams made of HSS or high-strength structural steel;
- Bending tests (three-point or four-point bending) reporting measured moment resistance or sufficient load-displacement data to compute M_{TEST};
- Complete geometric data: the depth (h), the flange width (b_f), the flange thickness (t_f), the web thickness (t_w), the unbraced length (L_b);
- Material properties with yield strength greater than or equal to 460 MPa, reported for the flange and/or web;
- Clear statement (or reconstructible description) of lateral restraint conditions so that L_b can be defined as above.

Exclusion rules

- Tests on singly-symmetric or channel/angle sections were excluded.
- Material properties with yield strength lower than 460 MPa reported for the flange and/or web.

Table 1 presents the database. Fig. 1 shows the range of each key parameter collected, considering the mean, standard deviation (SD), minimum and maximum. The database shows that only 1–5% of the specimens fall at the absolute limits for most geometric parameters (h, b_f, t_f, $f_{y,flange}$, $f_{y,web}$). Even under the broader criterion of percentiles (≤5% or ≥95%), the proportion remains modest (≈10-12%) for most parameters, except for the web thickness t_w (18%), reflecting the large number of thin-web specimens of HSS I-beams. Statistical outliers are rare, generally below 6%, again with t_w being the main exception (11.6%). These findings indicate that the database is dominated by intermediate parameter values.

It is important to note that the cross-sectional dimensions of all specimens fall within the limits prescribed by the design standards. According to by BS EN 1993-1-1, the sections may be classified as Class 1, 2, 3, or 4, depending on their susceptibility to local buckling. Under the ANSI/AISC 360-22 and AS 4100-1998 (R2020), the equivalent classifications are Compact, Non-compact, and Slender. The range of dimensions in the database therefore covers the full spectrum of permissible section classes in these specifications, ensuring that the results remain applicable across different design regimes and deformation limits. Consequently, the presence of a relatively small number of extreme-value specimens does not compromise the representativeness of the dataset nor the applicability of the code predictions evaluated in this study.

297 **Table 1: Database**

ID	Test	Ref.	h (mm)	b_f (mm)	t_f (mm)	t_w (mm)	L_b (mm)	Section type	$f_{y,flange}$ (MPa)	$f_{y,web}$ (MPa)	Load condition	M_{TEST} (kN.m)	Failure
1	1	(Dibley, 1969)	203.2	133.2	7.8	5.7	2944.1	Hot-rolled	505	505	UM	90.4	LTB
2	2	(Dibley, 1969)	203.2	133.2	7.8	5.7	2955.9	Hot-rolled	505	505	UM	83.9	LTB
3	3	(Dibley, 1969)	203.2	133.2	7.8	5.7	2639	Hot-rolled	505	505	UM	103.5	LTB
4	4	(Dibley, 1969)	203.2	133.2	7.8	5.7	2639	Hot-rolled	505	505	UM	102.5	LTB
5	7	(Dibley, 1969)	308.7	101.8	8.8	6.0	2639	Hot-rolled	516	516	UM	105.9	LTB
6	8	(Dibley, 1969)	308.7	101.8	8.8	6.0	2639	Hot-rolled	516	516	UM	96.8	LTB
7	9	(Dibley, 1969)	308.7	101.8	8.8	6.0	2303	Hot-rolled	516	516	UM	118.5	LTB

8	10	(Dibley, 1969)	308.7	101.8	8.8	6.0	2303	Hot-rolled	516	516	UM	126.3	LTB
9	11	(Dibley, 1969)	203.2	133.2	7.8	5.7	2065	Hot-rolled	505	505	UM	131.1	LTB
10	12	(Dibley, 1969)	203.2	133.2	7.8	5.7	2065	Hot-rolled	505	505	UM	130.6	LTB
11	13	(Dibley, 1969)	308.7	101.8	8.8	6.0	1463	Hot-rolled	516	516	UM	190.0	LTB
12	14	(Dibley, 1969)	308.7	101.8	8.8	6.0	1463	Hot-rolled	516	516	UM	180.8	LTB
13	15	(Dibley, 1969)	308.7	101.8	8.8	6.0	735	Hot-rolled	516	516	UM	217.4	LB
14	16	(Dibley, 1969)	308.7	101.8	8.8	6.0	735	Hot-rolled	516	516	UM	226.1	LB
15	17	(Dibley, 1969)	308.7	101.8	8.8	6.0	1029	Hot-rolled	516	516	UM	204.6	LTB
16	18	(Dibley, 1969)	308.7	101.8	8.8	6.0	1029	Hot-rolled	516	516	UM	235.6	LTB
17	19	(Dibley, 1969)	203.2	133.2	7.8	5.7	1302	Hot-rolled	505	505	UM	138.3	LTB

18	20	(Dibley, 1969)	203.2	133.2	7.8	5.7	1302	Hot-rolled	505	505	UM	130.7	LTB
19	21	(Dibley, 1969)	157.6	152.9	9.4	6.5	1512	Hot-rolled	581	581	UM	153.8	LTB
20	22	(Dibley, 1969)	157.6	152.9	9.4	6.5	1512	Hot-rolled	471	471	UM	127.3	LTB
21	23	(Dibley, 1969)	157.6	152.9	9.4	6.5	2940.2	Hot-rolled	462	462	UM	93.5	LTB
22	24	(Dibley, 1969)	157.6	152.9	9.4	6.5	3316.5	Hot-rolled	462	462	UM	83.4	LTB
23	27	(Dibley, 1969)	157.6	152.9	9.4	6.5	2517.2	Hot-rolled	468	468	UM	101.9	LTB
24	28	(Dibley, 1969)	157.6	152.9	9.4	6.5	2511.4	Hot-rolled	567	567	UM	114.0	LTB
25	30	(Dibley, 1969)	254.0	101.6	6.8	5.7	2268	Hot-rolled	463	463	UM	69.7	LTB
26	1	(McDermott, 1969)	202.4	223.0	9.4	7.5	304.8	Hot-rolled	862	862	UM	313.2	LB
27	2	(McDermott, 1969)	205.5	200.9	12.4	8.8	304.8	Hot-rolled	883	883	UM	473.8	LB

28	3	(McDermott, 1969)	211.8	170.2	14.1	9.8	304.8	Hot-rolled	793	793	UM	445.3	LB
29	4	(McDermott, 1969)	211.8	141.7	14.2	9.7	304.8	Hot-rolled	814	814	UM	398.7	LB
30	5	(McDermott, 1969)	211.6	113.0	14.1	9.8	304.8	Hot-rolled	820	820	UM	333.5	LB
31	6	(McDermott, 1969)	237.2	100.8	15.8	6.5	609.6	Welded	827	800	UM	353.8	LTB+LB
32	7	(McDermott, 1969)	238.3	150.9	15.7	6.8	914.4	Welded	820	800	UM	490.4	LTB+LB
33	A	(McDermott, 1969)	235.7	100.8	15.6	6.6	914.4	Welded	827	800	MG	387.3	LTB+LB
34	B	(McDermott, 1969)	234.4	151.6	15.7	6.6	1371.6	Welded	820	800	MG	532.0	LTB+LB
35	A1	(Beg and Hladnik, 1996)	246.7	300.2	12.5	10.4	1200	Welded	858	810	UM	684.0	LB
36	A2	(Beg and Hladnik, 1996)	245.7	298.7	12.4	10.4	1200	Welded	858	810	UM	673.2	LB
37	B1	(Beg and Hladnik, 1996)	247.5	271.0	12.4	10.4	1200	Welded	807	810	UM	643.0	LB

38	B2	(Beg and Hladnik, 1996)	246.0	269.3	12.5	10.4	1200	Welded	807	810	UM	645.4	LB
39	C1	(Beg and Hladnik, 1996)	246.5	251.0	12.6	10.4	1200	Welded	776	810	UM	616.4	LB
40	C2	(Beg and Hladnik, 1996)	247.7	250.8	12.7	10.4	1200	Welded	776	810	UM	623.5	LB
41	D1	(Beg and Hladnik, 1996)	245.7	220.8	12.4	10.4	1200	Welded	858	859	UM	604.7	LB
42	D2	(Beg and Hladnik, 1996)	246.2	220.4	12.4	10.4	1200	Welded	858	859	UM	605.2	LB
43	E1	(Beg and Hladnik, 1996)	245.9	198.8	12.6	10.4	1200	Welded	807	859	UM	572.0	LTB+LB
44	E2	(Beg and Hladnik, 1996)	247.8	199.0	12.6	10.4	1200	Welded	807	859	UM	572.9	LTB+LB
45	3	(Green *et al.*, 2002)	305.0	152.0	13.0	10.0	920	Welded	576	576	MG	511.3	LB
46	4A	(Green *et al.*, 2002)	534.0	152.0	13.0	10.0	920	Welded	609	609	MG	1094.0	LTB+LB
47	6	(Green *et al.*, 2002)	305.0	229.0	13.0	10.0	920	Welded	609	609	MG	722.1	LB

48	7	(Green *et al.*, 2002)	305.0	152.0	13.0	10.0	456	Welded	609	609	UM	507.1	LB
49	8	(Green *et al.*, 2002)	534.0	152.0	13.0	10.0	305	Welded	596	596	UM	1031.2	LB
50	HSB800-NC-LP-3	(Lee *et al.*, 2013)	400.0	500.0	17.6	17.6	3500	Welded	991	991	MG	3876.0	LB
51	HSB800-NC-LPD-3	(Lee *et al.*, 2013)	400.0	220.0	17.6	17.6	1160	Welded	991	991	MG	2334.3	TF
52	HSB800-C-LPD-3	(Lee *et al.*, 2013)	400.0	220.0	21.1	17.6	1160	Welded	879	991	MG	2546.1	TF
53	HSB800-NC-LP-4-A	(Lee *et al.*, 2013)	400.0	220.0	17.6	17.6	940	Welded	991	991	UM	2190.9	LTB
54	HSB800-NC-LP-4-B	(Lee *et al.*, 2013)	400.0	220.0	17.6	17.6	460	Welded	991	991	UM	2293.3	TF
55	HSA800-S-LPD-3-FHS	(Lee *et al.*, 2013)	400.0	650.0	17.6	17.6	4000	Welded	937	937	MG	3811.1	LB
56	HSA800-NC-LPD-3-PHS	(Lee *et al.*, 2013)	400.0	240.0	15.0	17.6	900	Welded	956	937	MG	2002.8	LB
57	HSA800-NC-LPD-3-FHS	(Lee *et al.*, 2013)	401.0	238.0	15.0	17.6	900	Welded	956	937	MG	2016.8	TF

		(Lee *et al.*, 2013)	400.	201.								2105.	
58	HSA800-C-LPD-3-PHS		0	0	20.0	17.6	900	Welded	903	937	MG	1	LB
		(Lee *et al.*, 2013)	399.	200.								2128.	
59	HSA800-C-LPD-3-FHS		0	0	20.0	17.6	900	Welded	903	937	MG	3	TF
		(Lee *et al.*, 2013)	400.	199.								2090.	
60	HSA800-C-LP-3-PHS		0	0	20.0	17.6	1430	Welded	903	937	MG	0	LB
		(Lee *et al.*, 2013)	400.	160.								1828.	LTB+L
61	HSA800-SC-LPD-3-PHS		0	0	20.0	17.6	702	Welded	903	937	MG	2	B
		(Lee *et al.*, 2013)	400.	160.								1860.	
62	HSA800-SC-LPD-3-FHS		0	0	20.0	17.6	702	Welded	903	937	MG	9	LB+TF
		(Lee *et al.*, 2013)	400.	241.								2027.	LTB+L
63	HSA800-NC-LP-4-PHS		0	0	15.0	17.6	900	Welded	956	937	UM	6	B
		(Lee *et al.*, 2013)	400.	240.								2021.	LTB+L
64	HSA800-NC-LP-4-FHS		0	0	15.0	17.6	900	Welded	956	937	UM	7	B
		(Lee *et al.*, 2013)	400.	199.								2033.	LTB+L
65	HSA800-C-LP-4-PHS		0	0	20.0	17.6	900	Welded	903	937	UM	0	B
		(Xiong *et al.*, 2016)	270.	179.									
66	C1		2	9	10.5	9.0	2500	Welded	525	541	MG	335.3	LTB
		(Xiong *et al.*, 2016)	268.	180.									
67	C2		7	0	10.5	9.0	3000	Welded	525	541	MG	326.4	LTB

68	C3	(Xiong *et al.*, 2016)	270.4	179.3	10.4	8.8	3500	Welded	525	541	MG	313.6	LTB
69	C4	(Xiong *et al.*, 2016)	271.1	180.1	10.4	8.7	4000	Welded	525	541	MG	272.9	LTB
70	C5	(Xiong *et al.*, 2016)	452.0	179.6	10.5	8.8	2500	Welded	525	541	MG	634.7	LTB
71	C6	(Xiong *et al.*, 2016)	451.2	180.0	10.4	8.9	3000	Welded	525	541	MG	580.8	LTB
72	C7	(Xiong *et al.*, 2016)	452.0	180.0	10.5	8.8	3500	Welded	525	541	MG	550.2	LTB
73	C8	(Xiong *et al.*, 2016)	448.2	180.7	10.5	8.4	4000	Welded	525	541	MG	487.2	LTB
74	B-52-1.5	(Yang *et al.*, 2019)	289.0	180.5	10.4	8.7	2160	Welded	525	541	MG	260.9	LTB
75	B-60-1.5	(Yang *et al.*, 2019)	270.7	180.7	10.4	8.7	2500	Welded	525	541	MG	216.1	LTB
76	B-72-1.5	(Yang *et al.*, 2019)	271.6	179.4	10.5	8.8	3000	Welded	525	541	MG	223.4	LTB
77	B-84-1.5	(Yang *et al.*, 2019)	271.7	180.3	10.5	9.0	3500	Welded	525	541	MG	189.8	LTB

78	B-64-2.0	(Yang *et al.*, 2019)	361.1	180.3	10.5	8.7	2500	Welded	525	541	MG	329.2	LTB
79	B-76-2.0	(Yang *et al.*, 2019)	360.1	180.5	10.5	8.9	3000	Welded	525	541	MG	287.8	LTB
80	B-89-2.0	(Yang *et al.*, 2019)	361.2	180.6	10.6	9.0	3500	Welded	525	541	MG	275.2	LTB
81	B-102-2.0	(Yang *et al.*, 2019)	362.0	180.6	10.4	8.9	4000	Welded	525	541	MG	368.0	LTB
82	H350-A	(Luo *et al.*, 2020)	350.0	150.0	12.0	10.0	1370	Welded	769	769	MG	802.8	LTB
83	I-690-1	(Le *et al.*, 2020)	354.0	159.5	11.8	7.7	3500	Welded	851	791	MG	478.0	LTB
84	I-690-2	(Le *et al.*, 2020)	353.5	159.3	11.8	7.7	750	Welded	851	791	UM	659.0	LB
85	I-690-3	(Le *et al.*, 2020)	354.3	160.0	11.8	7.7	3000	Welded	851	791	UM	509.0	LTB
86	I-890-1	(Le *et al.*, 2020)	353.5	159.9	11.8	8.0	3500	Welded	998	1003	MG	572.0	LTB
87	I-890-2	(Le *et al.*, 2020)	352.9	159.5	11.8	8.0	750	Welded	998	1003	UM	844.0	LB

88	I-890-3	(Le *et al.*, 2020)	354.0	160.2	11.8	8.0	3000	Welded	998	1003	UM	634.0	LTB
89	I-890-4	(Le *et al.*, 2020)	353.8	120.3	11.8	8.0	3000	Welded	998	1003	UM	330.0	LTB
90	I-890-5	(Le *et al.*, 2020)	254.5	120.2	11.8	8.0	3000	Welded	998	1003	UM	259.0	LTB
91	I-155-5-18-1	(Yan *et al.*, 2020)	202.0	101.9	10.1	10.9	5950	Welded	506	506	UM	68.5	LTB
92	I-155-5-18-2	(Yan *et al.*, 2020)	200.0	100.0	10.1	10.0	6032	Welded	506	506	UM	73.6	LTB
93	I-95-9-33-1	(Yan *et al.*, 2020)	350.5	179.5	10.1	10.6	6010	Welded	506	506	UM	303.5	LTB
94	I-95-9-33-2	(Yan *et al.*, 2020)	350.0	180.2	10.1	10.2	6028	Welded	506	506	UM	285.8	LTB
95	SA-HSB1	(Wang *et al.*, 2021)	262.0	112.0	10.0	6.0	600	Welded	784	720	MG	318.7	Y
96	SA-HSB2	(Wang *et al.*, 2021)	300.0	126.0	10.0	6.0	900	Welded	784	720	MG	398.2	Y
97	SA-HSB3	(Wang *et al.*, 2021)	380.0	170.0	10.1	6.0	900	Welded	784	720	MG	728.8	Y

98	SA-HSB4	(Wang *et al.*, 2021)	300.0	190.0	16.1	6.0	900	Welded	745	720	MG	843.3	Y
99	SB-HSB1	(Wang *et al.*, 2021)	262.0	112.2	10.1	6.0	1270	Welded	784	720	MG	319.7	LTB
100	SB-HSB2	(Wang *et al.*, 2021)	300.0	126.3	10.0	6.0	2100	Welded	784	720	MG	383.6	LTB
101	SB-HSB3-r	(Wang *et al.*, 2021)	430.0	170.1	10.1	6.0	2500	Welded	784	720	MG	710.0	LTB
102	SB-HSB4	(Wang *et al.*, 2021)	300.0	190.1	16.0	6.0	2700	Welded	745	720	MG	831.5	LTB
103	SC-HSB1	(Wang *et al.*, 2021)	262.0	112.2	9.9	6.0	1500	Welded	784	720	MG	282.8	LTB
104	SC-HSB2	(Wang *et al.*, 2021)	300.0	126.1	10.0	6.0	2700	Welded	784	720	MG	303.8	LTB
105	SC-HSB3-r	(Wang *et al.*, 2021)	430.0	170.1	10.0	6.0	3000	Welded	784	720	MG	444.8	LTB
106	SC-HSB4	(Wang *et al.*, 2021)	300.0	190.1	16.0	6.0	3300	Welded	745	720	MG	748.4	LTB
107	B1	(Tankova *et al.*, 2021)	498.9	201.0	16.2	8.6	2000	Welded	522	522	UM	779.4	LTB

10		(Tankova *et al.*,	498.	200.								1041.	
8	B2	2021)	0	3	15.7	8.3	2000	Welded	785	777	UM	9	LTB
10		(Tankova *et al.*,	496.	201.				Hot-					
9	B3	2021)	5	6	15.0	10.2	2000	rolled	484	470	UM	832.4	LTB
11		(Tankova *et al.*,	308.	298.									
0	B4	2021)	1	8	16.2	8.6	2000	Welded	522	522	UM	677.4	LTB
11		(Tankova *et al.*,	309.	300.								1024.	
1	B5	2021)	1	3	15.7	8.3	2000	Welded	785	777	UM	5	LTB
11		(Tankova *et al.*,	308.	296.				Hot-					
2	B6	2021)	5	5	14.9	8.5	2000	rolled	483	518	UM	725.1	LTB
11		(Tankova *et al.*,	745.	201.								1404.	
3	B7	2021)	4	7	15.8	8.3	2000	Welded	794	753	UM	9	LTB
11		(Tankova *et al.*,	746.	201.								1336.	
4	B8	2021)	2	3	15.8	8.1	2000	Welded	794	476	UM	3	LTB
11		(Xiong *et al.*, 2021)	271.	180.									
5	B-270-2.5		7	4	11.5	9.6	2500	Welded	786	788	MG	365.7	LTB
11		(Xiong *et al.*, 2021)	271.	181.									
6	B-270-3.0		7	1	11.6	9.4	3000	Welded	786	788	MG	328.1	LTB
11		(Xiong *et al.*, 2021)	270.	180.									
7	B-270-3.5		3	9	11.6	9.5	3500	Welded	786	788	MG	281.7	LTB

11		(Xiong *et al.*, 2021)	270.	181.								
8	B-270-4.0		1	1	11.6	9.6	4000	Welded	786	788	MG	256.4	LTB
11		(Xiong *et al.*, 2021)	449.	180.								
9	B-450-3.0		4	1	11.7	9.6	3000	Welded	786	788	MG	507.9	LTB
12		(Xiong *et al.*, 2021)	452.	180.								
0	B-450-3.5		1	2	11.7	9.6	3500	Welded	786	788	MG	407.3	LTB
12		(Xiong *et al.*, 2021)	452.	181.								
1	B-450-4.0		1	0	11.7	9.5	4000	Welded	786	788	MG	318.9	LTB
12		(Xiong *et al.*, 2021)	450.	181.								
2	B-450-4.5		6	0	11.6	9.9	4500	Welded	786	788	MG	274.5	LTB
12		(Xiong *et al.*, 2022)	350.	202.								
3	B350-0.50-1/3		4	3	13.6	9.7	2200	Welded	776	784	MG	878.0	LTB
12		(Xiong *et al.*, 2022)	350.	200.								
4	B350-0.75-1/3		6	7	13.6	9.7	2200	Welded	776	784	MG	860.0	LTB
12		(Xiong *et al.*, 2022)	347.	200.								
5	B350-1.00-1/3		8	4	13.6	9.6	2200	Welded	776	784	UM	818.0	LTB
12		(Xiong *et al.*, 2022)	347.	200.								
6	B350-0.50-1/4		7	7	13.6	9.7	3300	Welded	776	784	MG	849.0	LTB
12		(Xiong *et al.*, 2022)	348.	201.								
7	B350-0.75-1/4		3	7	13.6	9.7	3300	Welded	776	784	MG	811.0	LTB

128	B350-1.00-1/4	(Xiong *et al.*, 2022)	348.6	200.3	13.7	9.7	3300	Welded	776	784	UM	759.0	LTB
129	B450-0.50-1/3	(Xiong *et al.*, 2022)	450.6	201.9	13.7	9.5	2200	Welded	776	784	MG	1171.0	LTB
130	B450-0.75-1/3	(Xiong *et al.*, 2022)	449.9	198.9	13.7	9.6	2200	Welded	776	784	MG	1070.0	LTB
131	B450-1.00-1/3	(Xiong *et al.*, 2022)	448.8	200.8	13.7	9.6	2200	Welded	776	784	UM	1091.0	LTB
132	B450-0.50-1/4	(Xiong *et al.*, 2022)	450.0	200.0	14.0	10.0	3300	Welded	776	784	MG	864.0	LTB
133	B450-0.75-1/4	(Xiong *et al.*, 2022)	450.8	200.1	13.6	9.6	3300	Welded	776	784	MG	990.0	LTB
134	B450-1.00-1/4	(Xiong *et al.*, 2022)	451.3	200.7	13.6	9.6	3300	Welded	776	784	UM	939.0	LTB
135	HSS-I-65 × 116 × 8 × 8–3 PB	(Zhu *et al.*, 2023)	116.3	64.4	8.4	8.5	n/c*	Welded	783	783	MG	69.5	LB
136	HSS-I-65 × 116 × 8 × 8–3 PB-R	(Zhu *et al.*, 2023)	116.5	62.2	8.4	8.4	n/c*	Welded	783	783	MG	67.5	LB
137	HSS-I-80 × 136 × 8 × 8–3 PB	(Zhu *et al.*, 2023)	136.7	79.6	8.4	8.4	n/c*	Welded	783	783	MG	101.0	LB

13	HSS-I-80 × 136 × 8 × 8–3	(Zhu *et al.*, 2023)	136.										
8	PB-R		8	79.4	8.4	8.4	n/c*	Welded	783	783	MG	100.9	LB

*In these models, the unbraced length was very small due to a lateral brace system; UM and MG are Uniform Moment and Moment Gradient, respectively.

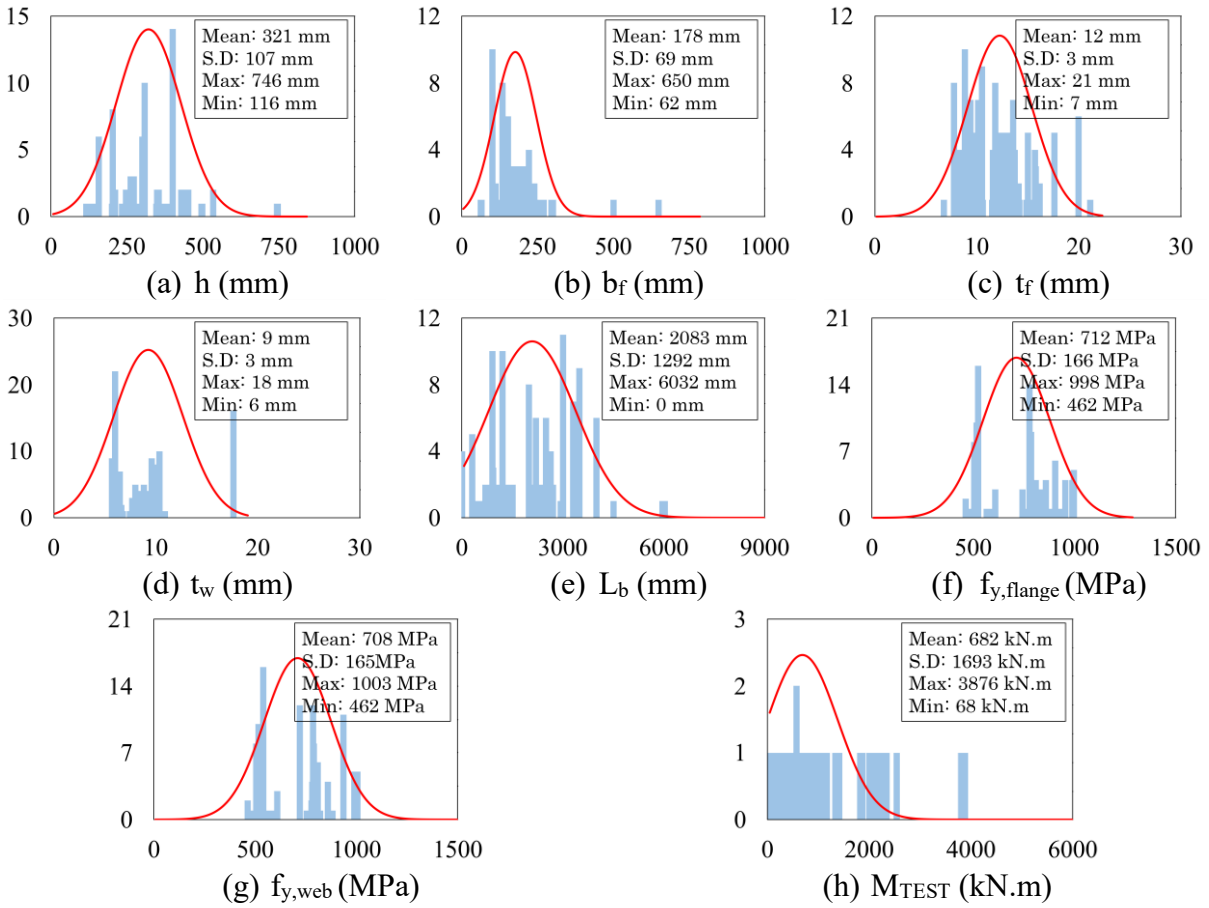


Fig. 1: Normal distribution of the database

3. Design codes

Design codes, like BS EN 1993-1-1 , ANSI/AISC 360-22 and AS 4100-1998 (R2020), apply the concept of classifying cross-sections to address the effects of local buckling (LB). Class 1 and Class 2 (Compact) sections can reach their complete plastic moment capacity in bending. In Class 3 (Non-compact) sections, LB takes place after the elastic moment is reached but before the plastic moment is achieved, limiting their bending resistance to the elastic moment capacity. In Class 4 (Slender) sections, local buckling occurs before the elastic moment is attained.

Regarding the consideration of residual stresses, each design standard adopts a distinct approach to account for the influence of residual stresses on member strength. For instance, ANSI/AISC 360-22 implicitly incorporates residual stresses by recommending the reduction of the yield moment capacity to $0.7f_y$, thereby limiting the contribution of the flange regions where compressive residual stresses are typically concentrated. BS EN 1993-1-1 considers imperfection factors that depend on the cross-section dimensions and fabrication process, influencing the member's buckling resistance curves. AS 4100-1998 (R2020), in turn, accounts for residual stresses in the definition of plate slenderness limits, which govern the classification of cross-sections and the applicability of elastic or plastic resistance models.

This section outlines the calculation methods for checking the LTB resistance of steel I-beams. It is important to emphasise that the equations presented in the design codes are based on the basic elastic critical moment ($M_{cr,0}$) (Timoshenko *et al.*, 1961).

3.1. BS EN 1993-1-1

The latest edition of BS EN 1993-1-1, released in 2022, offers two approaches for LTB resistance calculation: the General Method and a specific method for doubly symmetric I- and H-sections. In this study, this specific method will be referred to as the "New Method".

BS EN 1993-1-1 classification limits are calculated depending on the material parameter ($\varepsilon = \sqrt{235/f_y}$). These values are compared with the slenderness of the web (h_w/t_w) and flange ($0.5(b_f - t_w)/t_f$). The overall cross-section classification is established by the highest class from the checks performed.

3.1.1. General method

The design capacity of the LTB resistance (M_{Rd}) is calculated using Eqs. (1-5), in which M_{Rk} is the characteristic bending moment resistance, χ_{LT} is the reduction factor for LTB, λ_{LT} is the relative slenderness for LTB, α_{LT} is the imperfection factor for LTB, M_{cr} is the elastic critical moment, and W_y is the section modulus about the strong axis.

$$M_{Rk,EC3,GM} = \chi_{LT} M_{Rk} \tag{1}$$

$$\chi_{LT} = \frac{1}{\emptyset_{LT} + \sqrt{\emptyset_{LT}^2 - \lambda_{LT}^2}} \leq 1.0 \tag{2}$$

$$\emptyset_{LT} = 0.5[1 + \alpha_{LT}(\lambda_{LT} - 0.2) + \lambda_{LT}^2] \tag{3}$$

$$\lambda_{LT} = \sqrt{\frac{M_{Rk}}{M_{cr}}} \tag{4}$$

$$M_{Rk} = W_y f_y \tag{5}$$

The imperfection factor for LTB (α_{LT}) is equal to 0.21, 0.34, 0.49 and 0.76 for buckling curves ‘a’, ‘b’, ‘c’ and ‘d’, respectively. The selection of the buckling curve is influenced by the type of section and the h/b_f ratio, as shown in Table 2. According to section 8.3.2.3 from BS EN 1993-1-1, when $\lambda_{LT} \leq \lambda_{LT,0}$, the verification of LTB resistance may be neglected. $\lambda_{LT,0}$ is equal to 0.4 if end-fork support conditions are assumed.

340 **Table 2: Bucking curve selection for General Method**

Cross-section	Limits	Buckling curve
Hot-rolled	$h/bf \leq 2.0$	a
	$h/bf > 2.0$	b
Welded	$h/bf \leq 2.0$	c
	$h/bf > 2.0$	d

341

342 3.1.2. New method

343 The new BS EN 1993-1-1 proposal, which is based on the formulations studied by Taras and
344 Greiner (2010), for the calculation of LTB resistance is presented in Eqs. (6-9), in which f_M
345 factor can be taken as 1.0 as conservative, λ_z is the relative slenderness for flexural buckling
346 about the weak axis, $W_{y,el}$ is the elastic section modulus about the strong axis, $W_{z,el}$ is the elastic
347 section modulus about weak axis and L_z is the is the buckling length.

$$\chi_{LT} = \frac{f_M}{\emptyset_{LT} + \sqrt{\emptyset_{LT}^2 - f_M \lambda_{LT}^2}} \leq 1.0 \tag{6}$$

$$\emptyset_{LT} = 0.5\left\{1 + f_M\left[\frac{\lambda_{LT}^2}{\lambda_z^2}\alpha_{LT}(\lambda_z - 0.2) + \lambda_{LT}^2\right]\right\} \tag{7}$$

$$\lambda_z = \sqrt{\frac{A_i f_y}{N_{crz}}} \tag{8}$$

$$N_{crz} = \frac{\pi^2 E I_z}{L_z^2} \tag{9}$$

348 The imperfection factor (α_{LT}) for this method is presented in Table 3. For welded sections,
349 Tankova *et al.* (2022) recommended to reduce the factor from 0.21 to 0.16, considering high
350 strength steels. It improves accuracy by correcting the systematic underestimation of buckling
351 resistance observed in current BS EN 1993-1-1 provisions for high-strength steel members.
352 While the New Method refines the treatment of cross-section behaviour and buckling
353 resistance, Tankova *et al*. (2022)'s recalibration of the imperfection factors further reduces the
354 bias between predicted and observed resistances for both flexural and lateral-torsional buckling,

355 without compromising reliability. As a result, these approaches provide a more consistent and
356 realistic estimation of the capacity of HSS welded I-sections.

357 **Table 3: Imperfection factor selection for New Method, considering $t_f \leq 40$ mm**

Cross-section	Limits	α_{LT}
Hot-rolled	$h/bf > 1.2$	$0.12\sqrt{\frac{W_{el,y}}{W_{el,z}}} \leq 0.34$
	$h/bf \leq 1.2$	$0.16\sqrt{\frac{W_{el,y}}{W_{el,z}}} \leq 0.34$
Welded	-	$0.21\sqrt{\frac{W_{el,y}}{W_{el,z}}} \leq 0.64$

358

359 3.2. ANSI/AISC 360-22

360 The ANSI/AISC 360-22 limits for the section classification are presented in Table 4. In this
361 way, the nominal flexural strength of the flange (M_{nf}) is calculated via Eqs. (10-11), in which
362 M_{pl} is the plastic moment.

$$M_{nf} = \begin{cases} f_y W_{y,pl}, & b_f/2t_f \leq \lambda_{pf} \\ M_{pl} - \left(M_{pl} - 0.7 f_y W_{y,el}\right)\left(\frac{b_f/2t_f - \lambda_{pf}}{\lambda_{rf} - \lambda_{pf}}\right), & \lambda_{pf} < b_f/2t_f \leq \lambda_{rf} \\ \frac{0.9 E k_c W_{y,el}}{\left(b_f/2t_f\right)^2}, & \lambda_{rf} < b_f/2t_f \end{cases} \quad (10)$$

$$k_c = \frac{4}{\sqrt{h_w/t_w}}, 0.35 \leq k_c \leq 0.76 \quad (11)$$

363 The nominal flexural strength of the web (M_{nw}) is calculated via Eq. (12):

$$M_{nw} = \begin{cases} f_y W_{y,pl}, & h_w/t_w \leq \lambda_{pw} \\ M_{pl} - \left(M_{pl} - f_y W_{y,el}\right)\left(\frac{h_w/t_w - \lambda_{pw}}{\lambda_{rw} - \lambda_{pw}}\right), & \lambda_{pw} < h_w/t_w \leq \lambda_{rw} \end{cases} \quad (12)$$

364

365 **Table 4: Limits for flange and web classification**

Section	Flange		Web	
	Compact (λ_{pf})	Non-compact (λ_{rf})	Compact (λ_{pw})	Non-compact (λ_{rw})
Hot-rolled	$0.38\sqrt{\frac{E}{f_y}}$	$1.0\sqrt{\frac{E}{f_y}}$	$3.76\sqrt{\frac{E}{f_y}}$	$5.7\sqrt{\frac{E}{f_y}}$
Welded	$0.38\sqrt{\frac{E}{f_y}}$	$0.95\sqrt{\frac{k_c E}{0.7 f_y}}$		

366 The American Standard divides the LTB resistance into three ranges: plastic ($L_b \leq L_p$), inelastic
367 ($L_p < L_b \leq L_r$) and elastic ($L_r < L_b$). Unlike the inelastic and elastic regimes, in the plastic range,
368 LTB does not occur. These limits are calculated according to Eqs. (13-16), in which r_z is the
369 radius of gyration about the weak axis.

$$L_p = 1.76 r_z \sqrt{\frac{E}{f_y}} \tag{13}$$

$$L_r = 1.95 r_{ts} \frac{E}{0.7 f_y} \sqrt{\frac{J}{W_{y,el} h_o} + \sqrt{\left(\frac{J}{W_{y,el} h_o}\right)^2 + 6.76\left(\frac{0.7 f_y}{E}\right)^2}} \tag{14}$$

$$r_{ts}^2 = \frac{\sqrt{I_z C_w}}{W_{y,el}} \tag{15}$$

$$h_o = h - t_f \tag{16}$$

370 Then, the LTB resistance is calculated by Eq. (17).

$$M_{n,LTB} = \begin{cases} f_y W_{y,pl}, & L_b \leq L_p \\ C_b \left[M_{pl} - \left(M_{pl} - 0.7 f_y W_{y,el}\right)\left(\frac{L_b - L_p}{L_r - L_p}\right) \right], & L_p < L_b \leq L_r \\ C_b M_{cr,0}, & L_r < L_b \end{cases} \tag{17}$$

371 The coefficient C_b, shown in Eq. (18), is known as the modification factor for nonuniform
372 moment diagrams along the unbraced length (L_b). It is calculated according to Kirby and
373 Nethercot (1979).

$$C_b = \frac{12.5 M_{max}}{2.5 M_{max} + 3 M_A + 4 M_B + 3 M_C} \tag{18}$$

Finally, the characteristic resistance is determined by the lowest value of the three situations verified, as Eq. (19):

$$M_{Rk,AISC} = min\left(M_{nf}; M_{nw}; M_{n,LTB}\right) \quad (19)$$

3.3. AS 4100-1998 (R2020)

Regarding the cross-section classification of AS 4100-1998 (R2020), the section slenderness (λ_s) should be defined as the slenderness value (λ_e) of the plate element that exhibits the highest ratio of (λ_e/λ_{ey}) within the cross-section. The plate element slenderness of the flange and web is calculated according to Eqs. (20-21), respectively. The values of plate element slenderness limits are shown in Table 5. A heavily welded section is defined as one with compressive residual stress exceeding 40 MPa.

$$\lambda_{ef} = \frac{0.5\left(b_f - t_w\right)}{t_f}\sqrt{\frac{f_y}{250}} \quad (20)$$

$$\lambda_{ew} = \frac{h_w}{t_w}\sqrt{\frac{f_y}{250}} \quad (21)$$

Table 5: Plate element slenderness limits

	Residual stresses	Plasticity limit (λ_{ep})	Yield limit (λ_{ey})
Flange	Hot-rolled	9	16
(Uniform compression)	Heavy welded	8	14
Web	Hot-rolled	82	115
	Heavy welded		

In this way, if $\lambda_{ef}/\lambda_{eyf} > \lambda_{ew}/\lambda_{eyw}$, λ_{ef} is equal to λ_s. On the other hand, if $\lambda_{ew}/\lambda_{eyw} > \lambda_{ef}/\lambda_{eyf}$, λ_{ew} is equal to λ_s. Thus, the section modulus (W_y) is calculated according to Eq. (22). If $\lambda_s \leq \lambda_{ep}$, the section will be classified as compact. If $\lambda_{ep} < \lambda_s \leq \lambda_{ey}$, the section will be classified as non-compact. Finally, if $\lambda_{ey} < \lambda_s$, the section will be classified as slender.

$$W_y = \begin{cases} \min\left(W_{y,pl}; 1.5W_{y,el}\right), & \lambda_s \le \lambda_{ep} \\ W_{y,el} + \left[\min\left(W_{y,pl}; 1.5W_{y,el}\right) - W_{y,el}\right]\left(\dfrac{\lambda_{ey} - \lambda_s}{\lambda_{ey} - \lambda_{ep}}\right), & \lambda_{ep} < \lambda_s \le \lambda_{ey} \\ W_{y,el}\left(\dfrac{\lambda_{ey}}{\lambda_s}\right), & \lambda_{ey} < \lambda_s \end{cases} \quad (22)$$

The LTB resistance calculation presented in the Australian standard considers the loading position at cross-section height through the effective length (l_e), according to Eqs. (23-29). Considering Eq. (26), the AS 4100-1998 (R2020) defines γ_m equal 0.6. However, Le *et al.* (2020) proposed γ_m equal 0.7 for HSS I-beams with f_y>690 MPa.

$$M_{Rk,AS4100} = \alpha_m \alpha_s M_s \quad (23)$$

$$M_s = W_y f_y \quad (24)$$

$$\alpha_m = \frac{\sqrt{3}M_{max}}{\sqrt{(M_A)^2 + (M_B)^2 + (M_C)^2}} \le 2.5 \quad (25)$$

$$\alpha_s = \gamma_m\left(\sqrt{\lambda_s^4 + 3} - \lambda_s^2\right) \le 1 \quad (26)$$

$$\lambda_s = \sqrt{\frac{M_s}{M_o}} \quad (27)$$

$$M_o = \sqrt{\left\{\left(\frac{\pi^2 E I_y}{l_e^2}\right)\left[GJ + \left(\frac{\pi^2 E C_w}{l_e^2}\right)\right]\right\}} \quad (28)$$

$$l_e = k_t k_l k_r L \quad (29)$$

4. Results and discussion

This section evaluates the experimental data against the predicted results from various design standards, including BS EN 1993-1-1, ANSI/AISC 360-22 and AS 4100-1998 (R2020). The analysis focuses on the accuracy of each method in predicting the resistance across compact, non-compact, and slender high strength steel sections. Key statistical metrics, including mean ratios, regression coefficients, and errors, etc., are provided and discussed.

403 4.1. BS EN 1993-1-1

404 A comparison is made between the test data and the general method provided by BS EN 1993-
405 1-1. The I-beams are classified into Classes 1, 2, 3, and 4, and the results are plotted to show
406 the relationship between M_{TEST}/M_{Rk} on the vertical axis and $(M_{Rk}/M_{cr})^{0.5}$ on the horizontal axis,
407 according to Fig 2. These graphs are generated for buckling curves 'a', 'b', 'c', and 'd',
408 corresponding to different imperfection factors (α_{LT}) with values of 0.21, 0.34, 0.49, and 0.76,
409 respectively. As shown in Fig. 2a, the test data for Class 1 deviates from the predictions made
410 by the general method but aligns more closely with curve 'a' (i.e. with α_{LT}=0.21). Curves 'b',
411 'c', and 'd' are overly conservative for Class 1, showing a reduction in resistance earlier than
412 indicated by the test data. This suggests that curve 'a' is the most appropriate for predicting the
413 resistance of Class 1. For Class 2 (Fig. 2b), the general method with curve 'a' provides a good
414 agreement with some of the test data, though is conservative for other cases. Curve 'b' (i.e. with
415 α_{LT}=0.34) also yields similar predictions. However, curves 'c' and 'd' remain overly
416 conservative for most of the test data, leading to underestimation of the beam's resistance. In
417 the case of Class 3 (Fig. 2c), the general method using curves 'b' and 'c' provides reasonable
418 predictions for some of the test data but tends to be overly conservative for other cases. Curve
419 'd' is significantly too conservative for Class 3, underestimating the resistance in most cases.
420 For Class 4 (Fig. 2d), all curves 'a', 'b', 'c', and 'd' show varying degrees of discrepancy with
421 test data. The general method tends to overestimate the resistance in some cases while
422 underestimating it in others.

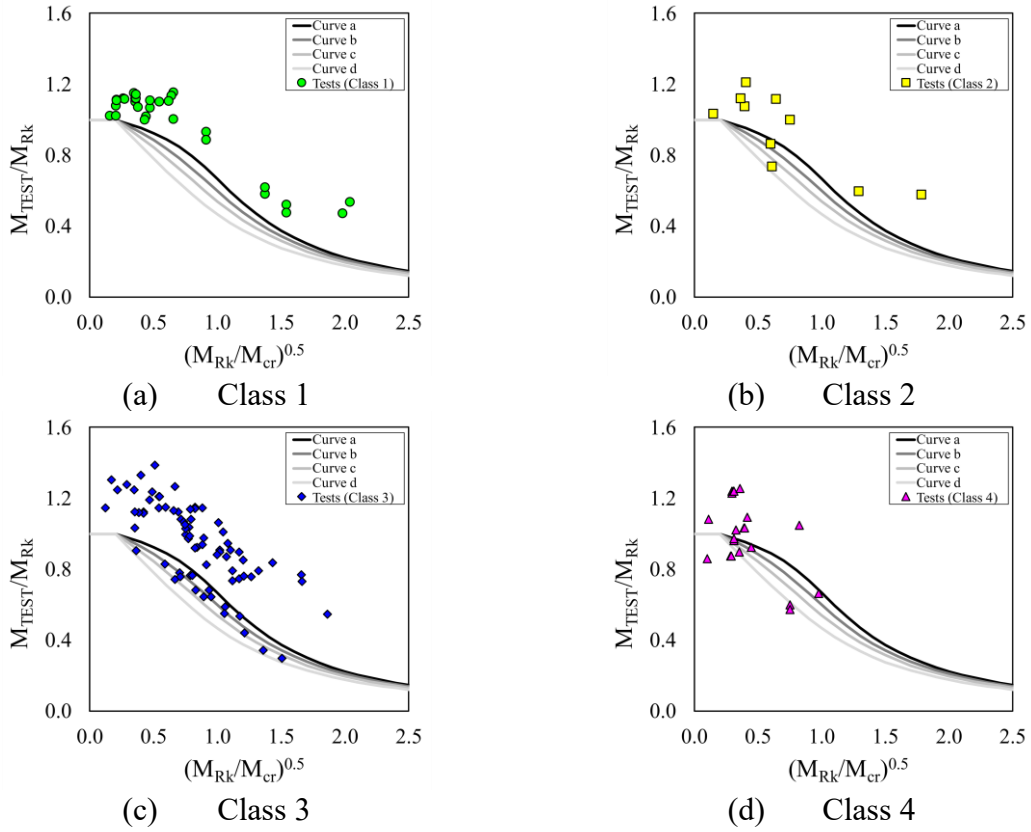
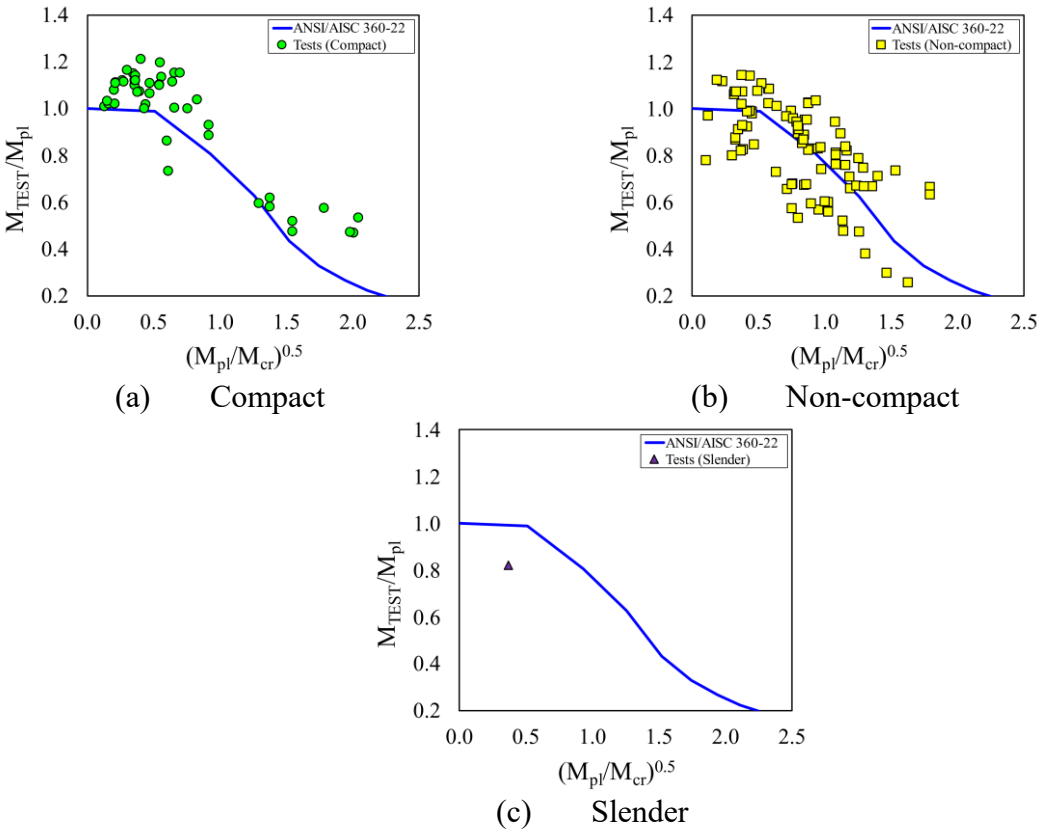


Fig. 2: BS EN 1993-1-1 General Method vs. tests

4.2. ANSI/AISC 360-22

This part compares the ratio of M_{TEST}/M_{pl} with $(M_{pl}/M_{cr})^{0.5}$ using the collected test data for compact, non-compact and slender HSS sections as specified in ANSI/AISC 360-22 (Fig. 3). This comparison aims to highlight the performance of this method in predicting the resistance. Hence, as depicted in Fig. 3a for compact sections, the plotted results show that the predicted values for M_{TEST}/M_{pl} are lower than the actual test data across most $(M_{pl}/M_{cr})^{0.5}$ values. This indicates that ANSI/AISC 360-22 tends to assume a lower resistance capacity than is observed practice for compact sections. In contrast, the results for non-compact sections display a more mixed performance (Fig. 3b). Approximately 49 of the test data for non-compact sections is overestimated (M_{Rk}/M_{TEST}>1.0) by the ANSI/AISC 360-22 method, while the 42 is underestimated (M_{Rk}/M_{TEST}<1.0). This discrepancy indicates that this method does not provide

436 a consistent predictive capacity for these sections. Regarding slender sections (i.e., flanges
437 slender and web compact), as shown in Fig. 3c, the ANSI/AISC 360-22 procedure
438 overestimates the resistance of HHS I-beams. It is important to highlight that the calculations
439 do not consider the coefficients Φ_{LFRD}=0.9 and Ω_{ASD}=1.67, considering the Load Resistance
440 Factor Design and Allowable Stress Design, respectively.



441 Fig. 3: ANSI/AISC 360-22 vs. tests
442
443 4.3. AS 4100-1998 (R2020)
444 The accuracy of the AS 4100-1998 (R2020) method is evaluated by comparing the ratio
445 M_{TEST}/M_s against $(M_s/M_o)^{0.5}$ using the collected test data for compact, non-compact, and slender
446 HSS sections (Fig. 4). The analysis summarises in Fig. 4a reveals that all collected test data for
447 compact sections (23 data points) fall above the AS 4100-1998 (R2020) curve, indicating that
448 the AS 4100-1998 (R2020) method tends to underestimate (M_{Rk}/M_{TEST}<1.0) the resistance of

these sections. For non-compact sections (Fig. 4b), the test data lies between the AS 4100-1998 (R2020) curve, with 75 data points being underestimated while the remaining others are overestimated. A similar trend is observed for slender sections (Fig. 4c), where the test data appears to lie between the AS 4100-1998 curve.

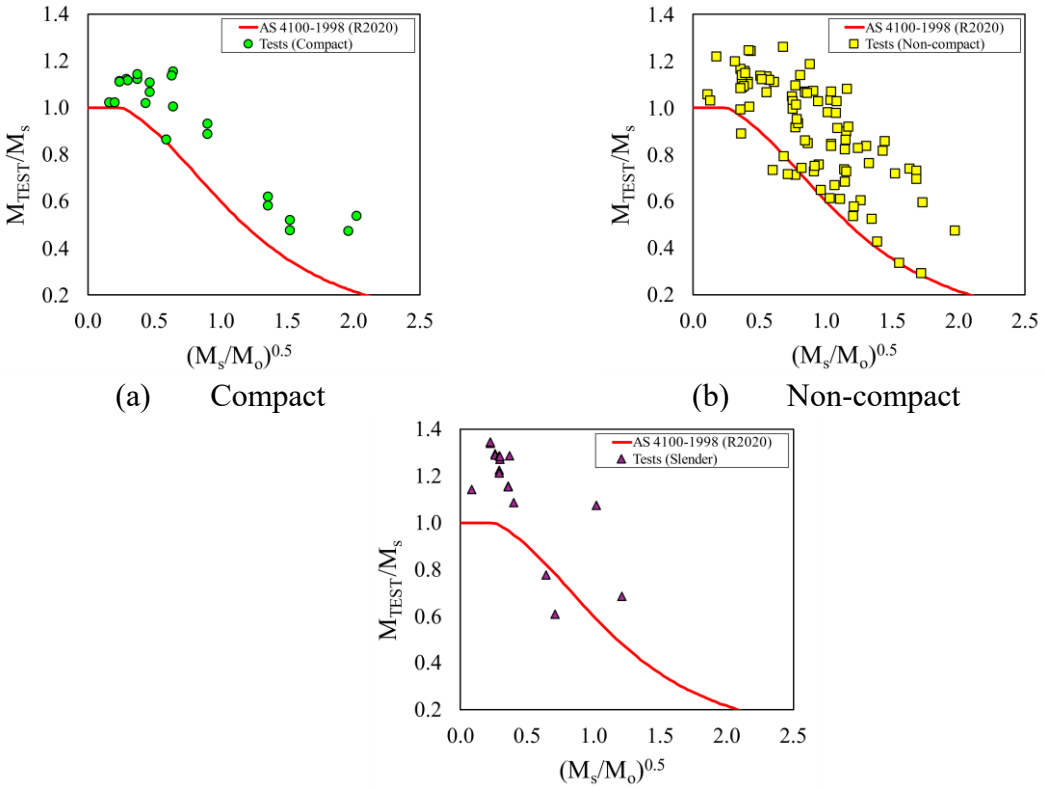


Fig. 4: AS 4100-1998 (R2020) vs. tests

4.4. Comparative analysis

The experimental data (M_{Test}) is compared with the predicted characteristic bending moment resistance (M_{Rk}) obtained from BS EN 1993-1-1 using both the general and new methods, as well as the new method combined with Tankova *et al.* (2022). Additionally, comparisons are made with predictions from ANSI/AISC 360-22 and AS 4100-1998 (R2020) and AS 4100-1998 (R2020) combined with Le *et al.* (2020).

461 The BS EN 1993-1-1 standard using the general method (Fig. 5a) underestimates
462 (M_{Rk}/M_{TEST}<1.0) the results in 128 cases and overestimates (M_{Rk}/M_{TEST}>1.0) the values in 10
463 cases. As shown in Table 7, the mean ratio of (M_{Rk}/M_{Test}), the SD, the CoV and the R^2 for this
464 method are 0.76, 19%, 25%, and 0.9366, respectively. The maximum and minimum relative
465 errors are 16.6% and -65.1%, respectively.

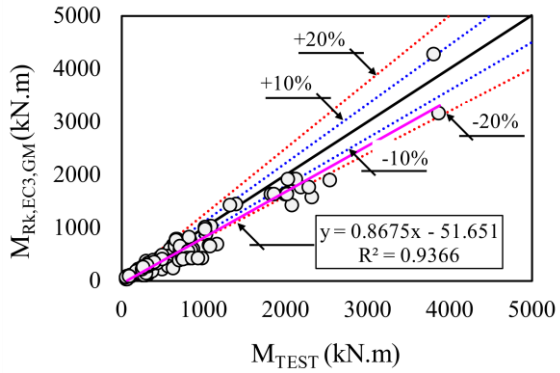
466 Similarly, for the BS EN 1993-1-1 standard using the new method (Fig. 5b), it underestimates
467 111 cases and overestimates 27 observations. According to Table 7, the mean ratio of
468 (M_{Rk}/M_{Test}), the SD, the CoV and the R^2 are 0.84, 19%, 22%, and 0.9453, respectively, with
469 maximum and minimum relative errors of 18.9% and -63.6%.

470 For the BS EN 1993-1-1 new method combined with Tankova *et al.* (2022) (Fig. 5c), the
471 method underestimates 110 cases and overestimates 28 observations. The mean ratio of
472 (M_{Rk}/M_{Test}), the SD, the CoV and the R^2 are 0.86, 20%, 23%, and 0.9483, respectively. The
473 maximum and minimum relative errors are 28.8% and -61.6%. Overall, the statistical results
474 across all methods are quite similar, reflecting their comparable performance. However, the BS
475 EN 1993-1-1 new method combined with Tankova *et al.* (2022) provides the most accurate
476 estimations.

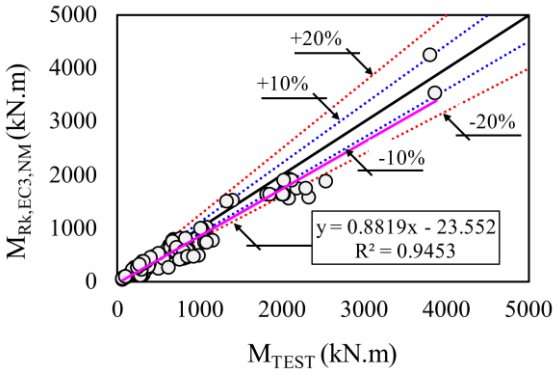
477 For ANSI/AISC 360-22 (Fig. 5d), it underestimates 101 cases and overestimates 27 cases. The
478 mean ratio of (M_{Rk}/M_{Test}), the SD, the CoV and the R^2 are 0.98, 24%, 25%, and 0.8846,
479 respectively. The maximum and minimum relative errors are 67.38% and -55.2%. This
480 indicates that BS EN 1993-1-1 offers a more accurate estimation compared to ANSI/AISC 360-
481 22.

482 Regarding AS 4100-1998 (R2020) (Fig. 5e), it provides conservative predictions for 114 cases,
483 and non-conservative for 24 cases. The mean ratio of (M_{Rk}/M_{Test}), the SD, the CoV and the R^2

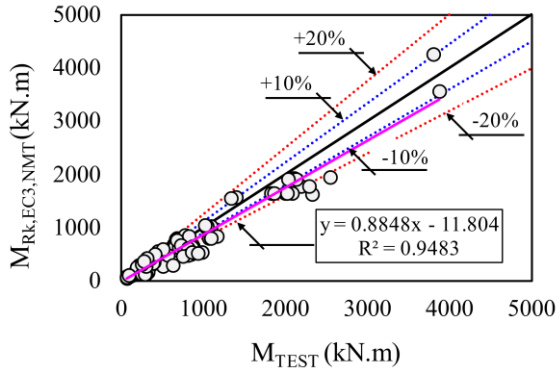
are 0.86, 22%, 25%, and 0.8791, respectively. The maximum and minimum relative errors are 41.8% and -60.5%. Now, analysing the combination of AS 4100-1998 (R2020) with Le *et al.* (2020), 112 observations are underestimated, while 26 are overestimated. For this combination, the mean ratio of (M_{Rk}/M_{Test}), the SD, the CoV and the regression coefficient R^2 are 0.90, 24%, 27%, and 0.8575, respectively. The maximum and minimum relative errors are 65.4% and -60.5%.



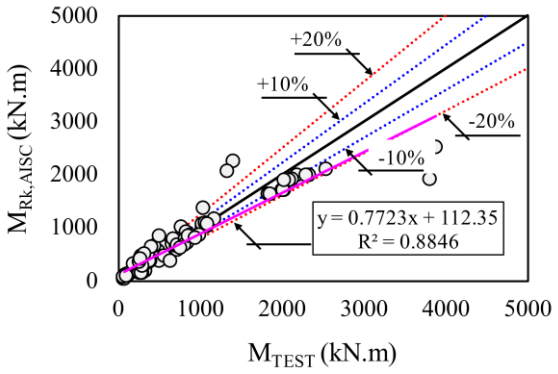
(a) General Method



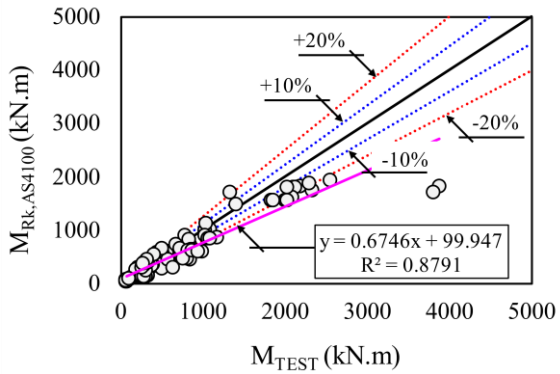
(b) New Method



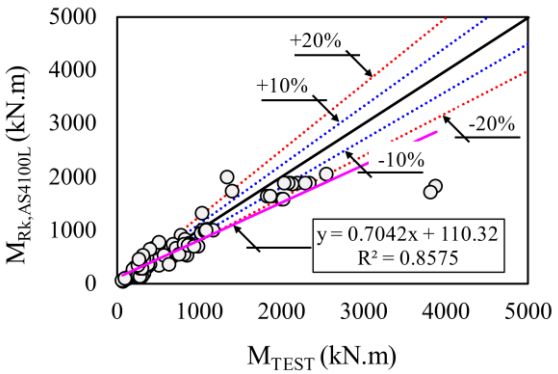
(c) New Method and Tankova *et al.* (2022)



(d) ANSI/AISC 360-22



(e) AS 4100-1998 (R2020)



(f) AS 4100-1998 (R2020) and Le *et al.* (2022)

Fig. 5: Comparative analysis between design codes and tests

Table 6 presents additional statistical metrics for each design method, including the Root Mean Square Error (RMSE) and Mean Absolute Error (MAE). This information further confirms that the BS EN 1993-1-1 new method, combined with Tankova *et al.* (2022), provides the most accurate estimations, evidenced by the lowest MAE and RMSE values.

The discrepancies in predictions among the three considered design standards are mainly due to the mechanical assumptions considered in each method and the parameters calibration. For instance, in BS EN 1993-1-1, the predicted LTB resistance depends strongly on the choice of buckling curve associated with the different imperfection factor (α_{LT}), which may influence the effect of initial geometric imperfections and residual stresses. ANSI/AISC 360-22 provides limits defining compact, non-compact, and slender elements using a particular set of data, hence, the interaction between flange and web slenderness and the higher yield strengths of HSS may not be fully captured, leading to inconsistent predictions, particularly for non-compact and slender elements. Similarly, AS 4100-1998 (R2020) generally provides conservative predictions for compact sections and shows variable accuracy for non-compact and slender sections, this may be influenced by the assumptions regarding section slenderness and residual stresses, particularly in heavily welded members. Among the examined methods, the BS EN 1993-1-1 new method with the Tankova *et al.* (2022) adjustment provides the most reliable and consistent predictions across all section types, as it incorporates updated imperfection factors and a more representative model for HSS I-beam behaviour. Overall, the mechanical basis of each design standard (i.e. imperfections, residual stresses, section slenderness effects, and plasticity development) explains the observed differences in prediction accuracy.

514 **Table 6: Statistical analysis of comparative study (M_{Rk}/M_{TEST})**

	General Method	**New Method**	**New Method and** Tankova *et al.* (2022)	**ANSI/AISC 360-22**	**AS 4100-1998 (R2020)**	**AS 4100-1998 (R2020) and** Le *et al.* (2020)
Mean	0.76	0.84	0.86	0.99	0.86	0.90
SD	0.19	0.19	0.20	0.24	0.22	0.24
CoV	0.25	0.22	0.23	0.25	0.25	0.27
R^2	0.9366	0.9453	0.9483	0.8846	0.8791	0.8575
MAE (kN.m)	155.4	126.5	121.2	117.4	153.9	143.1
RMSE (kN.m)	230.4	198.0	187.2	253.3	309.7	300.1
Minimum error	-65.1%	-63.6%	-61.6%	-55.21%	-60.5%	-60.5%
Maximum error	16.6%	18.9%	28.8%	67.3%	41.8%	65.4%

515
516
517
518
519
520
521
522

5. Sensitivity analysis

In the previous section, a competitive analysis is performed to assess the predictions of resistance for HSS doubly symmetric I-beams in accordance with different design methods available in international design standards including BS EN 1993-1-1, ANSI/AISC 360-22 and AS 4100-1998 (R2020). These methods are found to provide over-conservative predictions in most cases and do not offer a straightforward design procedure. Therefore, in this section, a new expression is developed based on the collected experimental data using a Multiple Non-linear Regression Analysis to predict the resistance for HSS doubly symmetric I-beams, compromising neither the practicality nor the accuracy.

The analysis is developed using Multiple Regression with Logarithmic Transformations to simplify the non-linear relationships into to linear relationships and allow for determination of the indices. The data is then fitted into a multiple linear regression model and the expression is converted back to the original power-law form. The analysis includes the most influential parameters including the depth (h), the flange width (b_f), the flange thickness (t_f), the web thickness (t_w), the unbraced length (L_b), the yield strength of the flange ($f_{y,flange}$), and the yield strength of the web ($f_{y,web}$). To ensure both methodological rigor and engineering applicability, a regression-based approach was adopted as it enables clear interpretation of parameter influence while maintaining dimensional consistency through logarithmic transformations. These transformations allowed the non-linear relationships to be expressed in linear form without compromising physical relevance or compatibility among variables. To further validate the robustness of the regression-based expression and avoid overfitting, k-fold cross-validation was employed as part of the analysis process. This approach was selected because it allows all data to be used efficiently for both training and validation, rather than relying on a single split that may introduce sampling bias. The dataset was divided into equal subsets, and the model was trained and tested iteratively across these partitions to assess its stability and predictive

548 accuracy – an approach particularly suitable in structural engineering research, where datasets
549 are often limited and parameter sensitivity is high. The cross-validation results confirmed that
550 the regression expression produced consistent predictions across all iterations, while confidence
551 interval checks verified the statistical relevance of the coefficients. Moreover, a comparison
552 with existing predictive formulations demonstrated lower MAE and RMSE values, indicating
553 that the proposed expression provides reliable accuracy and practical applicability for resistance
554 estimation within the defined parameter range. The expression for predicting resistance (M_{Reg})
555 is presented in Eq. (30), for the range of parameters given in Table 1.

$$M_{Reg} = 1.61 \times 10^{-5} \times (h)^{1.156} \times (b_f)^{0.93} \times (t_f)^{1.168} \times (t_w)^{0.052} \times (L_b)^{-0.256} \times (f_{y,flange})^{0.176} \times (f_{y,web})^{0.536} \quad (30)$$

556 Fig. 6 presents the results obtained from the regression expression in comparison with the tests.
557 As shown in the results, the regression expression results in an underestimation of 80 cases and
558 an overestimation of 58 cases. The performance of the regression expression is found to be
559 stable and capable of providing excellent resistance predictions compared with the other design
560 methods given in global design standards in terms of accuracy, precision, and consistency, as
561 presented in Table 5. The mean ratio of (M_{Reg}/M_{Test}), the standard deviation (SD), the coefficient
562 of variation (CoV) and the regression coefficient (R^2) are 1.02, 24%, 23%, and 0.9489,
563 respectively. The maximum and minimum relative errors are 65.8% and -32.1%.

564 As shown in the results, the regression expression exhibits excellent performance in several key
565 metrics. It has the highest mean value of the predicted-to-test ratio among the other design
566 methods with a slight overestimation of the resistance. It also maintains a low value of standard
567 deviation (SD) and coefficient of variation (CoV) which are consistent with other methods,
568 particularly ANSI/AISC 360-22 and AS 4100-1998 (R2020). In terms of the accuracy and

errors, the regression expression has shown outstanding performance with the lowest values of MAE and RMSE, confirming better precision and accuracy.

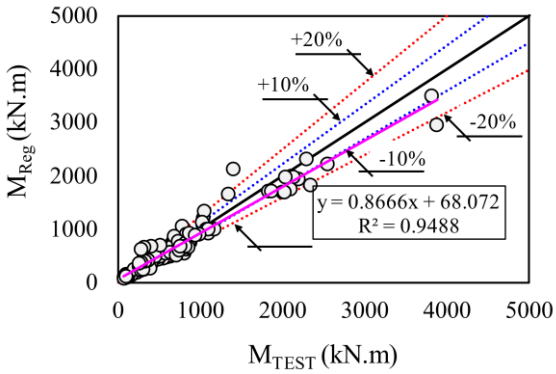
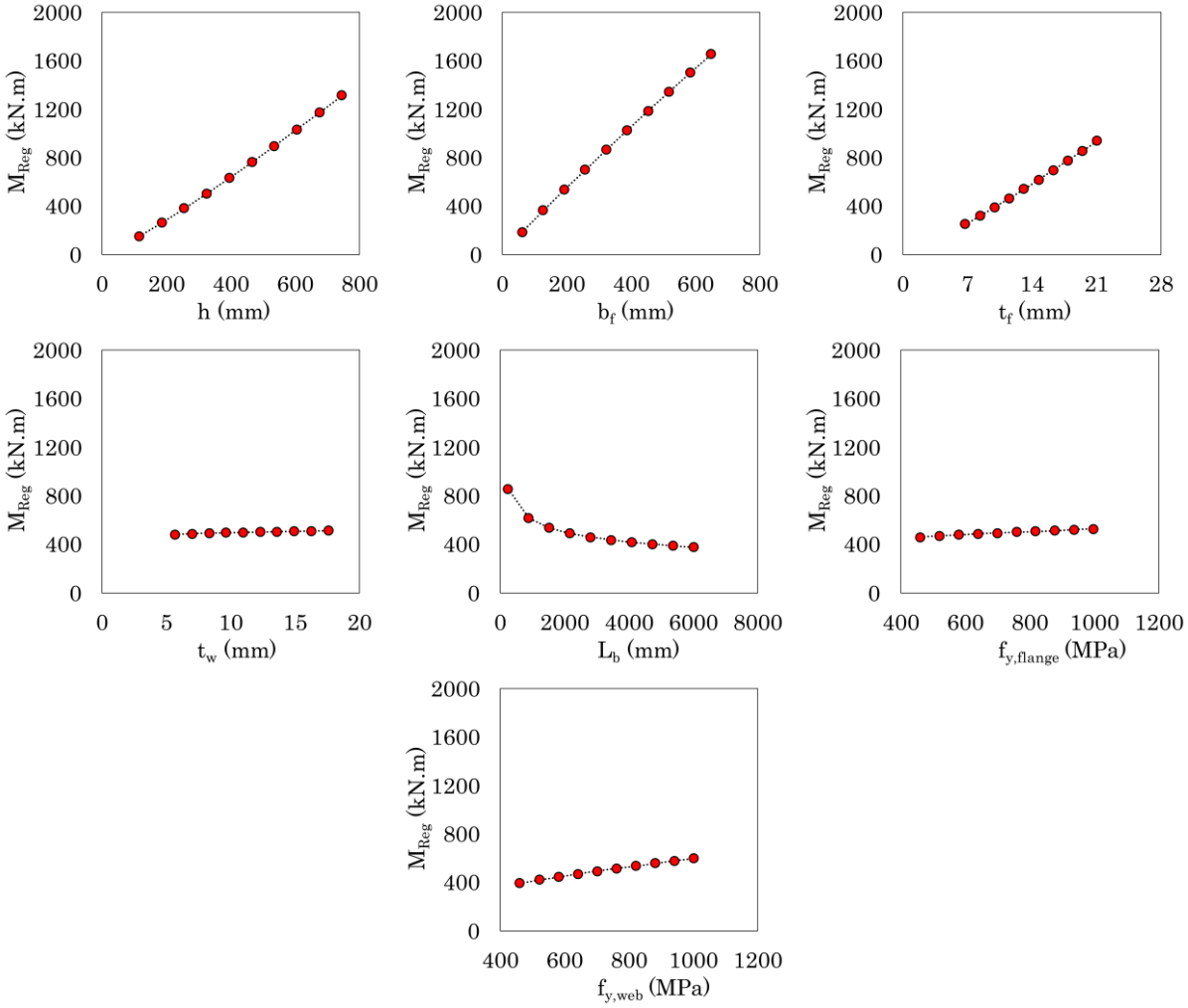


Fig. 6: Comparative analysis between the regression expression and tests

The influence of the key parameters is assessed based on the regression expression given in Eq. (30), as presented in Fig. 7. The sensitivity analysis includes the most influential parameters, particularly the depth (Fig. 7a), the flange width (Fig. 7b) and thickness (Fig. 7c), the web thickness (Fig. 7d), the unbraced length (Fig. 7e), the yield strength for the flange (Fig. 7f) and for the web (Fig. 7g). It is observed from the results that the parameters (h), (b_f), (t_f), and ($f_{y,web}$) have a strong positive effect on the resistance of HSS doubly symmetric I-beams, while the parameters ($f_{y,flange}$) and (t_w) show a very slight positive contribution towards the resistance. This is theoretically accepted since the flange fails in most cases prior to reaching the yield strength capacity. On the other hand, the unbraced length (L_b) demonstrates a non-linear inverse relationship, suggesting a strong negative impact on the resistance. Although flange yield strength ($f_{y,flange}$) is generally expected to influence flexural resistance, its low sensitivity in the present analysis can be explained by the dominant role of geometric stiffness parameters such as depth (h) and flange width (b_f), which govern the moment of inertia and resistance to lateral-torsional buckling. Once adequate flange dimensions are present, further increases in material strength have a limited effect on the overall response, as the failure mode is stiffness-controlled rather than purely strength-driven. Additionally, the web contributes to torsional and shear

589 stability, which explains why ($f_{y,web}$) shows slightly higher influence despite its lower overall
590 percentage. Therefore, the results do not contradict fundamental mechanics but rather reflect
591 the interaction between geometry and material properties within the parameter ranges
592 investigated.



593 Fig. 7: The influence of the key parameters on resistance

594 The sensitivity of each individual parameter on the resistance is calculated using Eq. (31) by
595 keeping all other parameters at their average value, in which f_{max} and f_{min} denote the highest and
596 lowest estimated value (Shamass *et al.*, 2023).

$$SA_i = \frac{f_{max}(x_i) - f_{min}(x_i)}{\sum_1^n [f_{max}(x_i) - f_{min}(x_i)]} 100 \quad (31)$$

The findings of the sensitivity analysis are depicted in Fig. 8. The results highlight that the flange width (b_f) has the highest significant influence followed by the height (h) with a sensitivity score of 35.9% and 28.3%, respectively. A moderate influence is observed for the unbraced length (L_b), flange thickness (t_f), the yield strength of the web ($f_{y,web}$) with a sensitivity score of 16.8 %, 11.7% and 5.1%, respectively. In contrast, the web thickness (t_w) and the yield strength of the flange ($f_{y,flange}$) demonstrate insignificance influence with a sensitivity score of 0.7 % and 1.6%, respectively.

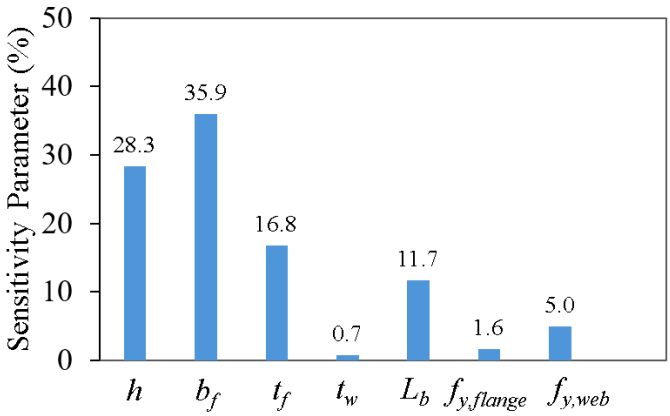


Fig. 8: The sensitivity of the key parameters on the resistance

6. Reliability analyses

This section presents a reliability analysis conducted in accordance with Annex D of EN 1990 to evaluate the reliability of the formulations, which were presented in Sections 3 and 4, and to present a partial safety factor for the resistance of HSS doubly symmetric I-beams. The statistical evaluation of the BS EN 1993-1-1 General Method, BS EN 1993-1-1 New Method, BS EN 1993-1-1 New Method combined with Tankova *et al.* (2022), ANSI/AISC 360-22 and AS 4100-1998 (R2020), and AS 4100-1998 (R2020) combined with Le *et al.* (2020) prediction model is developed herein based on the collected test data.

615 The product $b\delta_i$ for each experimental value must be calculated using Eq. (32), in which $r_{e,i}$, $r_{t,i}$,
616 b and δ_i are the experimental resistance, theoretical resistance, the mean value correction factor,
617 and the error result for each experimental resistance, respectively.

$$b\delta_i = \frac{r_{e,i}}{r_{t,i}} \tag{32}$$

618 The estimated value of $\bar{\Delta}$ is taken, according to Eq. (33-34), in which Δ_i is logarithm of the error
619 term $b\delta_i$.

$$\bar{\Delta} = \frac{1}{n}\sum_{i=1}^{n}\Delta_i \tag{33}$$

$$\Delta_i = \ln(b\delta_i) = \ln(r_{e,i}) - \ln(r_{t,i}) \tag{34}$$

620 The coefficient of variation of the error term δ_i can be calculated using Eqs. (35-36):

$$V_\delta = \sqrt{\exp(s_\Delta^2) - 1} \tag{35}$$

$$s_\Delta^2 = \frac{1}{n-1}\sum_{i=1}^{n}(\Delta_i - \bar{\Delta})^2 \tag{36}$$

621 The mean value correction factor b is determined by Eq. (37):

$$b = exp\left(\bar{\Delta} + \frac{1}{2}s_\Delta^2\right) \tag{37}$$

622 The coefficient of variation V_r can be estimated from Eqs. (38-39), in which V_{Xi} is the coefficient
623 of variation for yield strength of steel. It also applies for the geometric dimensions of the beam.

$$V_r^2 = \left(V_\delta^2 + 1\right)\left[\prod_{i=1}^{j}(V_{Xi}^2 + 1)\right] - 1 \quad (38)$$

$$V_{rt}^2 = \sum_{i}^{j} V_{Xi}^2 \quad (39)$$

624 The characteristic resistance r_k (n>100) is obtained from Eqs. (40-41), in which k_∞ is the value
625 of k_n for n→∞ (k_∞=1.64).

$$r_k = bg_{rt}\left(\underline{X_m}\right)\exp\left(-k_\infty Q - 0.5Q^2\right) \quad (40)$$

$$Q = \sqrt{ln(V_r^2 + 1)} \quad (41)$$

626 Design value r_d (n>100) is derived from Eq. (42), in which $k_{d,\infty}$ is the value of $k_{d,n}$ for n→∞
627 ($k_{d,\infty}$=3.04).

$$r_d = bg_{rt}\left(\underline{X_m}\right)\exp\left(-k_{\mathrm{d},\infty}Q - 0.5Q^2\right) \quad (42)$$

628 Thus, the partial factor (γ_{M0}) is calculated by Eq. (43):

$$\gamma_{M0} = \frac{r_k}{r_d} \quad (43)$$

629 Table 7 presents the main statistical parameters, which include the number of data (n), the
630 design fractile factor ($k_{d,n}$), the characteristic fractile factor (k_n), the average ratio of test to
631 resistance model predictions based on the least squares fit to the data ($\bar{b}$), the combined
632 coefficient of variation incorporating both resistance model and basic variable uncertainties
633 (V_r), and the partial safety factor for resistance (γ_{M0}). The CoV for the geometric dimensions
634 of the steel beam is 0.02, while the CoV for both normal and high-strength steel materials was

635 assumed to be 0.055 (Shamass and Guarracino, 2020). By implementing the First Order
636 Reliability Method (FORM) according to the Eurocode target reliability standards, the partial
637 factors (γ_{M0}) were assessed for all models. The FORM method utilises specific well-established
638 approximations, yielding results that are generally regarded as adequately accurate for most
639 structural applications.

640 The reliability assessment is carried out to meet a target reliability index of β greater than 3.8,
641 corresponding to a failure probability below 1×10^{-4} over a 50-year reference period. This
642 reliability level is achieved by applying suitable design fractile factors $k_{d,n}$ for the ultimate limit
643 state.

644 **Table 7: Overview of the reliability analysis performed in accordance with EN**
645 **1990**

Resistance model	n	$\bar{b}$	$k_{d,n}$	k_n	V_δ	V_r	γ_{M0}
General Method	138	1.413	3.04	1.64	0.2838	0.291	1.490
New Method		1.271	3.04	1.64	0.2559	0.264	1.438
New Method and Tankova *et al.* (2022)		1.232	3.04	1.64	0.2539	0.262	1.434
ANSI/AISC 360-16		1.078	3.04	1.64	0.2483	0.256	1.423
AS 4100-1998		1.242	3.04	1.64	0.2635	0.271	1.452
AS 4100-1998 and Le *et al.* (2020)		1.190	3.04	1.64	0.2696	0.278	1.463

646 The BS EN 1993-1-1 General Method, with a partial safety factor of 1.490, exhibited the highest
647 safety margin and reflects conservative design. This aligns with the findings of Rebelo *et al.*
648 (2009), who noted that the BS EN 1993-1-1 General method provides conservative results but
649 exhibits significant variability, particularly when the LTB reduction factor approaches unity.
650 On the other hand. The BS EN 1993-1-1 New Method and BS EN 1993-1-1 New Method
651 combined with Tankova *et al.* (2022), with partial safety factors of 1.438 and 1.434
652 respectively, showed slightly lower conservatism compared to the BS EN 1993-1-1 General
653 Method but remained within Eurocode 3's reliability framework. In contrast to the General

Method, the New Method calculates the imperfection factor based on the geometry of the cross section. However, according to Tankova *et al.* (2022), reducing the imperfection factors from 0.21 to 0.16 enhances accuracy.

In contrast, the ANSI/AISC 360-22 method, with a partial safety factor value of 1.423, represented the least conservative approach. This observation aligns with previous findings. As illustrated in Fig. 2, most test results exceed the buckling curve 'a' of BS EN 1993-1-1.

The AS 4100-1998 (R2020) formulations showed partial safety factors of 1.452 and 1.463, depending on whether the design included the contributions from Le *et al.* (2020). These values are slightly lower than the BS EN 1993-1-1 General Method but higher than the ANSI/AISC 360-22. This indicates that the AS 4100-1998 (R2020) standard maintains a moderate level of conservatism. Incorporating the refinements proposed by Le *et al.* (2020) results in a slight increase in the factor, indicating a potential adjustment to improve reliability in certain HSS applications.

Overall, the calibrated (γ_{M0}) values are consistent with typical outcomes of Eurocode code-calibration procedures: higher variability or model uncertainty results in larger partial factors, while more accurate formulations yield lower, but still acceptable values. All proposed factors therefore align with practical design needs and satisfy the reliability objectives of EN 1990.

Conclusions

This study evaluated the bending resistance of HSS doubly symmetric I-beams based on 138 experimental results reported between 1969 and 2023 and assessed the predictive accuracy of AS 4100-1998 (R2020), ANSI/AISC 360-22, and BS EN 1993-1-1, including recent refinements proposed in the literature. A parameter influence analysis was conducted using the collected data, followed by a reliability assessment.

677 The results showed that all standards tend to underestimate the resistance of HSS I-beams,
678 although to different extents. Among the Eurocode-based formulations, the BS EN 1993-1-1
679 New Method combined with the adjustments proposed by Tankova *et al.* (2022) provided the
680 most accurate estimates, with the highest R^2 and reduced variability. ANSI/AISC 360-22
681 exhibited the least conservative predictions, while AS 4100-1998 (R2020) presented a moderate
682 level of conservatism, slightly reduced when incorporating the refinements by Le *et al.* (2020).
683 The reliability analysis confirmed these trends, with partial safety factors ranging from 1.423
684 (ANSI/AISC 360-22) to 1.490 (BS EN 1993-1-1 General Method), highlighting systematic
685 differences in conservatism between codes.

686 A parameter-influence analysis showed that geometric properties-particularly depth (h), flange
687 width (b_f), flange thickness (t_f), and web yield strength ($f_{y,web}$) are the main contributors to the
688 resistance of HSS doubly symmetric I-beams, while flange yield strength ($f_{y,flange}$) and web
689 thickness (t_w) have only minor effects. The unbraced length (L_b) has a strong negative influence.
690 These trends are consistent with stiffness-governed behavior, in which geometry dominates
691 moment capacity and lateral-torsional stability, limiting the influence of increased material
692 strength within the tested parameter range. Therefore, the observed parameter sensitivities
693 remain consistent with structural mechanics and reflect the interaction between geometry and
694 material properties within the parameter range investigated.

695 The study has its own limitations. First, the database is heterogeneous, spanning more than five
696 decades, multiple research groups, and differing steel grades, testing procedures, and cross-
697 sectional configurations. Second, the analysis relied exclusively on previously published
698 experiments; therefore, some parameters could not be controlled or standardised, which may
699 affect the robustness of conclusions for extremely high-strength steels.

Nevertheless, the findings provide meaningful implications for the design of HSS I-beams. The consistent conservatism observed in current codes, especially in Eurocode-based methods, suggests opportunities for refinement, particularly in the calibration of imperfection factors and the treatment of cross-section geometry in LTB resistance predictions. These insights support ongoing efforts to adapt design provisions to modern high-strength steels and can assist practitioners in selecting code approaches that balance safety and accuracy.

Declaration of funding

This study was financed in part by the Conselho Nacional de Desenvolvimento Cientifico e Tecnológico (CNPq), grant number #404719/2023-6.

References

Alpsten, G.A. (1968), "Thermal residual stresses in hot-rolled steel members. Fritz Laboratory Reports No. 337.3, Lehigh University, Bethlehem, Pennsylvania".

Alpsten, G.A. and Tall, L. (1970), "Residual stresses in heavy welded shapes", *Welding Journal (AWS)*, Vol. 49, pp. 93–105.

American Institute of Steel Construction. (2010), "ANSI/AISC 360-10 - Specification for structural steel buildings.", Chicago.

American Institute of Steel Construction. (2016), "ANSI/AISC 360-16 - Specification for structural steel buildings.", Chicago.

720 American Institute of Steel Construction. (2022), “ANSI/AISC 360-22 - Specification for
721 structural steel buildings.”, Chicago.

722 Ban, H., Shi, G., Bai, Y., Shi, Y. and Wang, Y. (2013), “Residual stress of 460 MPa high
723 strength steel welded i section: Experimental investigation and modeling”, *International*
724 *Journal of Steel Structures*, Vol. 13 No. 4, pp. 691–705, doi: 10.1007/s13296-013-4010-
725 1.

726 Beer, H. and Schultz, G. (1970), “Theoretical basis for the European column curves”,
727 *Construction Métallique* , Vol. 3, p. 58.

728 Beg, D. and Hladnik, L. (1996), “Slenderness limit of Class 3 I cross-sections made of high
729 strength steel”, *Journal of Constructional Steel Research*, Vol. 38 No. 3, pp. 201–217, doi:
730 10.1016/0143-974X(96)00025-9.

731 Bjorhovde, R. (2004), “Development and use of high performance steel”, *Journal of*
732 *Constructional Steel Research*, Vol. 60 No. 3–5, pp. 393–400, doi: 10.1016/S0143-
733 974X(03)00118-4.

734 Dibley, J.E. (1969), “Lateral torsional buckling of I-sections in grade 55 steel”, *Proceedings of*
735 *the Institution of Civil Engineers*, Vol. 43 No. 4, pp. 599–627, doi:
736 10.1680/iicep.1969.7315.

737 European Committee for Standardization. (2002), “EN 1993-1-1: Eurocode 3 – Design of steel
738 structures – Part 1-1: General rules and rules for buildings”, Brussels.

739 European Committee for Standardization. (2022), “EN 1993-1-1: Eurocode 3 – Design of steel
740 structures – Part 1-1: General rules and rules for buildings”.

741 Galambos, T. V. and Ketter, R.L. (1959), "Columns under combined bending and thrust",
742 *Journal of the Engineering Mechanics Division*, Vol. 85 No. 2, pp. 1–30.

743 Galambos, T. V. and Surovek, A.E. (2008), *Structural Stability of Steel: Concepts and*
744 *Applications for Structural Engineers*, John Wiley & Sons, Inc, New Jersey.

745 Green, P.S., Sause, R. and Ricles, J.M. (2002), "Strength and ductility of HPS flexural
746 members", *Journal of Constructional Steel Research*, Vol. 58 No. 5–8, pp. 907–941, doi:
747 10.1016/S0143-974X(01)00102-X.

748 Huber, A.W. and Beedle, L.S. (1954), "Residual stress and the compressive strength of steel .
749 Welding Journal, 33 (12), p. 589-s, (December 1954), Reprint No. 96 (54-3)", *Fritz*
750 *Laboratory Reports*.

751 Jönsson, J. and Stan, T.-C. (2017), "European column buckling curves and finite element
752 modelling including high strength steels", *Journal of Constructional Steel Research*, Vol.
753 128, pp. 136–151, doi: 10.1016/j.jcsr.2016.08.013.

754 Karabulut, B., Ferraz, G. and Rossi, B. (2021), "Lifecycle cost assessment of high strength
755 carbon and stainless steel girder bridges", *Journal of Environmental Management*, Vol.
756 277, p. 111460, doi: 10.1016/j.jenvman.2020.111460.

757 Kirby, P. and Nethercot, D. (1979), *Design for Structural Stability*, Granada Publishing,
758 Suffolk.

759 Le, T., Bradford, M.A., Liu, X. and Valipour, H.R. (2020), "Buckling of welded high-strength
760 steel I-beams", *Journal of Constructional Steel Research*, Vol. 168, p. 105938, doi:
761 10.1016/j.jcsr.2020.105938.

762 Lee, C.-H., Han, K.-H., Uang, C.-M., Kim, D.-K., Park, C.-H. and Kim, J.-H. (2013), "Flexural
763 Strength and Rotation Capacity of I-Shaped Beams Fabricated from 800-MPa Steel",
764 *Journal of Structural Engineering*, Vol. 139 No. 6, pp. 1043–1058, doi:
765 10.1061/(ASCE)ST.1943-541X.0000727.

766 Li, T.-J., Li, G.-Q. and Wang, Y.-B. (2015), "Residual stress tests of welded Q690 high-strength
767 steel box- and H-sections", *Journal of Constructional Steel Research*, Vol. 115, pp. 283–
768 289, doi: 10.1016/j.jcsr.2015.08.040.

769 Luo, J., Zong, S., Zhu, S., Guo, X. and Yu, M. (2020), "Mechanical behavior of Q690 high-
770 strength steel beams at room and elevated temperatures", *The Structural Design of Tall*
771 *and Special Buildings*, Vol. 29 No. 5, doi: 10.1002/tal.1712.

772 McDermott, J.F. (1969), "Plastic Bending of A514 Steel Beams", *Journal of the Structural*
773 *Division*, Vol. 95 No. 9, pp. 1851–1871, doi: 10.1061/JSDEAG.0002351.

774 Mela, K. and Heinisuo, M. (2014), "Weight and cost optimization of welded high strength steel
775 beams", *Engineering Structures*, Vol. 79, pp. 354–364, doi:
776 10.1016/j.engstruct.2014.08.028.

777 Miki, C., Homma, K. and Tominaga, T. (2002), "High strength and high performance steels
778 and their use in bridge structures", *Journal of Constructional Steel Research*, Vol. 58 No.
779 1, pp. 3–20, doi: 10.1016/S0143-974X(01)00028-1.

780 Nagaraja Rao, N.R., Estuar, F.R. and Tall, L. (1964), "Residual stresses in welded shapes. Fritz
781 Laboratory Reports No 249.18. Lehigh University, Bethlehem, Pennsylvania."

782 Rabi, M., Ferreira, F.P.V., Abarkan, I., Limbachiya, V. and Shamass, R. (2023), "Prediction of
783 the cross-sectional capacity of cold-formed CHS using numerical modelling and machine
784 learning", *Results in Engineering*, Vol. 17, p. 100902, doi: 10.1016/j.rineng.2023.100902.

785 Rabi, M., Jweihan, Y.S., Abarkan, I., Ferreira, F.P.V., Shamass, R., Limbachiya, V.,
786 Tsavdaridis, K.D., *et al.* (2024), "Machine learning-driven web-post buckling resistance
787 prediction for high-strength steel beams with elliptically-based web openings", *Results in*
788 *Engineering*, Vol. 21, p. 101749, doi: 10.1016/j.rineng.2024.101749.

789 Rebelo, C., Lopes, N., Simões da Silva, L., Nethercot, D. and Vila Real, P.M.M. (2009),
790 "Statistical evaluation of the lateral–torsional buckling resistance of steel I-beams, Part 1:
791 Variability of the Eurocode 3 resistance model", *Journal of Constructional Steel Research*,
792 Vol. 65 No. 4, pp. 818–831, doi: 10.1016/j.jcsr.2008.07.016.

793 Ricles, J.M., Sause, R. and Green, P.S. (1998), "High-strength steel: implications of material
794 and geometric characteristics on inelastic flexural behavior", *Engineering Structures*, Vol.
795 20 No. 4–6, pp. 323–335, doi: 10.1016/S0141-0296(97)00024-2.

796 Sabau, G., Lagerqvist, O. and Baddoo, N. (2020), "Statistical Analysis of Flexural-Buckling-
797 Resistance Models for High-Strength Steel Columns", *Journal of Structural Engineering*,
798 Vol. 146 No. 2, doi: 10.1061/(ASCE)ST.1943-541X.0002529.

799 Schaper, L., Tankova, T., Simões da Silva, L. and Knobloch, M. (2022), "A novel residual
800 stress model for welded I-sections", *Journal of Constructional Steel Research*, Vol. 188,
801 p. 107017, doi: 10.1016/j.jcsr.2021.107017.

802 Shamass, R., Abarkan, I. and Ferreira, F.P.V. (2023), "FRP RC beams by collected test data:
803 Comparison with design standard, parameter sensitivity, and reliability analyses",
804 *Engineering Structures*, Vol. 297, p. 116933, doi: 10.1016/j.engstruct.2023.116933.

805 Shamass, R. and Guarracino, F. (2020), "Numerical and analytical analyses of high-strength
806 steel cellular beams: A discerning approach", *Journal of Constructional Steel Research*,
807 Vol. 166, p. 105911, doi: 10.1016/j.jcsr.2019.105911.

808 Shi, G., Zhu, X. and Ban, H. (2016), "Material properties and partial factors for resistance of
809 high-strength steels in China", *Journal of Constructional Steel Research*, Vol. 121, pp.
810 65–79, doi: 10.1016/j.jcsr.2016.01.012.

811 Spoorenberg, R.C., Snijder, H.H. and Hoenderkamp, J.C.D. (2011), "Proposed residual stress
812 model for roller bent steel wide flange sections", *Journal of Constructional Steel*
813 *Research*, Vol. 67 No. 6, pp. 992–1000, doi: 10.1016/j.jcsr.2011.01.009.

814 Standards Association of Australia. (2016), "AS 4100-1998 Steel Structures", Sydney,
815 Australia.

816 Standards Association of Australia. (2020), "AS 4100-1998 Steel Structures", Sydney.

817 Su, A., Sun, Y., Liang, Y. and Zhao, O. (2021), "Membrane residual stresses and local buckling
818 of S960 ultra-high strength steel welded I-section stub columns", *Thin-Walled Structures*,
819 Vol. 161, p. 107497, doi: 10.1016/j.tws.2021.107497.

820 Szalai, J. and Papp, F. (2005), "A new residual stress distribution for hot-rolled I-shaped
821 sections", *Journal of Constructional Steel Research*, Vol. 61 No. 6, pp. 845–861, doi:
822 10.1016/j.jcsr.2004.12.004.

823 Tall, L. (1961), *The Strength of Welded Built-up Columns. PhD Diss.*, Lehigh University.

824 Tankova, T., Rodrigues, F., Leitão, C., Martins, C. and Simões da Silva, L. (2021), "Lateral-
825 torsional buckling of high strength steel beams: Experimental resistance", *Thin-Walled*
826 *Structures*, Vol. 164, p. 107913, doi: 10.1016/j.tws.2021.107913.

827 Tankova, T., Simões da Silva, L. and Rodrigues, F. (2022), "Buckling curve selection for HSS
828 welded I-section members", *Thin-Walled Structures*, Vol. 177, p. 109430, doi:
829 10.1016/j.tws.2022.109430.

830 Taras, A. and Greiner, R. (2010), "New design curves for lateral-torsional buckling-Proposal
831 based on a consistent derivation", *Journal of Constructional Steel Research*, Vol. 66 No.
832 5, pp. 648–663, doi: 10.1016/j.jcsr.2010.01.011.

833 Timoshenko, S., Gere, J. and Timoshenko, S. (1961), *Theory of Elastic Stability*, 2nd ed.,
834 McGraw-Hill Book Company, New York, N. Y.

835 Veljkovic, M. and Johansson, B. (2004), "Design of hybrid steel girders", *Journal of*
836 *Constructional Steel Research*, Vol. 60 No. 3–5, pp. 535–547, doi: 10.1016/S0143-
837 974X(03)00128-7.

838 Wang, K., Xiao, M., Chung, K.-F. and Nethercot, D.A. (2021), "Lateral torsional buckling of
839 partially restrained beams of high strength S690 welded I-sections", *Journal of*
840 *Constructional Steel Research*, Vol. 184, p. 106777, doi: 10.1016/j.jcsr.2021.106777.

841 Wang, W. and Qin, S. (2016), "Experimental investigation of residual stresses in thin-walled
842 welded H-sections after fire exposure", *Thin-Walled Structures*, Vol. 101, pp. 109–119,
843 doi: 10.1016/j.tws.2016.01.005.

844 Wheeler, A. and Russell, B. (2005), "Behaviour and design of webs in high strength steel under
845 flexural loading", *Fourth International Conference on Advances in Steel Structures*,
846 Elsevier, pp. 137–142, doi: 10.1016/B978-008044637-0/50018-4.

847 Xiong, G., Feng, Y., Liao, X.-D., Gu, Y. and Kang, S.-B. (2022), "Lateral–torsional buckling
848 behaviour of welded Q690 steel I-beams with double lateral restraints along the length",
849 *Thin-Walled Structures*, Vol. 170, p. 108659, doi: 10.1016/j.tws.2021.108659.

850 Xiong, G., Feng, Y., Peng, Q., Kang, S.-B., Zhang, Y. and Fan, Y.-L. (2021), "Lateral-torsional
851 buckling behaviour of 690 MPa high strength steel beams", *Structures*, Vol. 33, pp. 3999–
852 4010, doi: 10.1016/j.istruc.2021.06.085.

853 Xiong, G., Kang, S.-B., Yang, B., Wang, S., Bai, J., Nie, S., Hu, Y., *et al.* (2016), "Experimental
854 and numerical studies on lateral torsional buckling of welded Q460GJ structural steel
855 beams", *Engineering Structures*, Vol. 126, pp. 1–14, doi:
856 10.1016/j.engstruct.2016.07.050.

857 Yan, X.-L., Li, G.-Q., Wang, Y.-B. and Jiang, J. (2020), "Experimental and numerical
858 investigation on flexural-torsional buckling of Q460 steel beams", *Journal of*
859 *Constructional Steel Research*, Vol. 174, p. 106276, doi: 10.1016/j.jcsr.2020.106276.

860 Yang, B., Nie, S., Xiong, G., Hu, Y., Bai, J., Zhang, W. and Dai, G. (2016), "Residual stresses
861 in welded I-shaped sections fabricated from Q460GJ structural steel plates", *Journal of*
862 *Constructional Steel Research*, Vol. 122, pp. 261–273, doi: 10.1016/j.jcsr.2016.03.029.

863 Yang, B., Zhang, Y., Xiong, G., Elchalakani, M. and Kang, S.-B. (2019), "Global buckling
864 investigation on laterally-unrestrained Q460GJ steel beams under three-point bending",
865 *Engineering Structures*, Vol. 181, pp. 271–280, doi: 10.1016/j.engstruct.2018.12.028.

866 Young, B.W. (1975), “Residual stresses in hot rolled members”, *IABSE*, Vol. 23, doi:
867 http://doi.org/10.5169/seals-19798.

868 Zhu, Y., Yun, X. and Gardner, L. (2023), “Behaviour and design of high strength steel
869 homogeneous and hybrid welded I-section beams”, *Engineering Structures*, Vol. 275, p.
870 115275, doi: 10.1016/j.engstruct.2022.115275.

871